Beam-Beam Effects in Tevatron Run II

V.Shiltsev, Y.Alexahin, V.Lebedev, P.Lebrun, R.S.Moore, T.Sen, A.Tollestrup, A.Valishev, X.L.Zhang

Fermi National Accelerator Laboratory, PO Box 500, Batavia, IL 60510, USA

Abstract

The Tevatron in Collider Run II (2001-present) is operating with six times more bunches, many times higher beam intensities and luminosities than in Run I (1992-1995). Electromagnetic long-range and head-on interactions of high intensity proton and antiproton beams have been significant sources of beam loss and lifetime limitations. We present observations of the beam-beam phenomena in the Tevatron and results of relevant beam studies. We analyze the data and various methods employed in operations, predict the performance for planned luminosity upgrades, and discuss ways to improve it.

PACS numbers: 29.27.bd

1. INTRODUCTION: COLLIDER RUN II LUMINOSITY AND BEAM PARAMETER

Run II of the Tevatron proton-antiproton collider began in March 2001. Compared to Run I, the beam energy was increased from 900 GeV to 980 GeV and the number of bunches was increased from 6 to 36 in each beam, in order to increase luminosity many times above the Run I record peak luminosity of 0.25 10^{32} $cm^{-2}s^{-1}$. Since the start of Run II, the Tevatron peak luminosity has steadily improved and reached the level of 1.2 10^{32} $cm^{-2}s^{-1}$ (see Fig. 1) - significantly exceeding the original Run IIa peak luminosity goal [1] without using electron cooling of antiprotons in the Recycler Ring (RR). The progress was a result of more than a dozen improvements in the injectors and the Tevatron itself, each giving a 5-25% performance increase. The improvements have often been introduced during regular shutdown periods (8-12 weeks long every autumn). Details of the accelerator complex operations can be found in Ref. [1] and descriptions of the numerous improvements are given in [2]. More than 1 fb^{-1} of integrated luminosity has been delivered to each of the CDF and D0 experiments

to date. In parallel to the Collider operation, we have started a luminosity upgrade project which should lead to peak luminosities of about 2.7 10^{32} $cm^{-2}s^{-1}$ and total integrated luminosity of 4.4-8.5 fb^{-1} through 2009. Table 1 contains various parameters of the Tevatron beams for present operation and their design values after the planned luminosity upgrades.

Figure 2 presents a typical Tevatron operation cycle. A collider fill starts with 150 GeV proton bunches from the Main Injector injected one bunch at a time onto the central orbit of the Tevatron. The bunches are loaded in three trains of 12 bunches each, with 396 ns bunch separation and 2.6 μs gaps between the trains. Protons and antiprotons circulate in the same beam pipe, so electrostatic separators are used to put the beams onto separate helical orbits. After all 36 proton bunches are loaded, the separators are powered to put the protons on their helical orbit. Antiprotons are loaded onto the antiproton helical orbit, four bunches at a time, into one of the three abort gaps. The antiproton bunches are moved longitudinally relative to the proton bunches ("cogged") to make room for the next four bunches in the abort gap. In Fig. 2, the coggings are marked by (artificial) spikes in the antiproton bunch intensity caused by instrumentation effects. After injection, the two beams are accelerated to 980 GeV in about 85 seconds. A final cogging is done a few seconds after the ramp. Then, the optics are changed in 25 steps to reduce the beta functions at the interaction points (IPs) from 1.6 m to 0.35 m. After the final step of this "low-beta squeeze", the beams are brought into collision at the IPs by using separators around the IPs. Next, a dozen collimators are inserted to reduce the beam halo background in the detectors. A high energy physics (HEP) store begins shortly thereafter.

It should be noted that because of the way the injection complex operates, the antiprotons bunches vary significantly in intensity and emittance. As an example, Fig. 3 shows parameters of all antiproton and proton bunches at the start of store #3692 (July 31, 2004). Proton bunch intensities and emittances vary from bunch to bunch by less than 5%, while antiproton bunch intensities vary by a factor of 3, and emittances by a factor of 1.5. The transverse emittances cited in this paper are 95% normalized emittances which relate to the RMS beam sizes $\sigma_{x,y}$ as $\varepsilon_{x,y} = 6\beta\gamma(\sigma_{x,y}{}^2 - D_{x,y}^2(\delta p/p)^2)/\beta_{x,y}$, where $\delta p/p$ is the RMS momentum spread, and $\beta_{x,y}$ and $D_{x,y}$ are the beta and dispersion functions, respectively. Most of the variations have a period of 12 and 4: the intensities and transverse emittances of bunches at the end of each train are typically smaller than those at the beginning of the trains. Consequently, the instantaneous luminosity per bunch crossing can differ by a factor of 3 or more.

One can see in Fig. 2 that minor beam losses occur at every step of the Tevatron cycle. Some losses are intentional, like the few percent loss of protons and antiprotons during the halo removal process. Such scraping greatly reduces background event rates in both detectors and improves their data-taking efficiency. The beam losses during injection, ramp and squeeze phases are mostly caused by beam-beam effects. Since the start of Run II, these losses have been reduced greatly, as demonstrated in Fig. 4, such that the total beam intensity loss in the Tevatron prior to initiating collisions is currently ≈16%. Details on that subject will be presented below. In "proton-only" or "antiproton-only" stores, the losses do not exceed 2-3% per specie. So, the remaining 10-12% loss is caused by beam-beam effects. The proton and antiproton inefficiencies are similar, despite the factor of 6-10 difference in intensity.

Figure 5 shows the decay of instantaneous CDF luminosity over store #3657. The solid line represents the result of a simplified two parameter fit:

$$L(t) = \frac{L_0}{1 + t/\tau_L} \tag{1}$$

with an initial luminosity L_0=1.12 10^{32} $cm^{-2}s^{-1}$ and an initial luminosity lifetime τ_L=6.1 hr. The empirical fit works satisfactorily and reveals that the luminosity lifetime $(dL/dt \ / \ L)^{-1}$ grows approximately linearly over time from τ_L=6-8 hr to some 25-30 hr at the end of the T=30-hour long store. From Eq. (1) one can calculate the integrated luminosity for a store to be $L_0\tau_L\ln(1+ T /\tau_L)$. For long stores $T >> \tau_L$ (the average Tevatron store duration in 2004-2005 was about 23 hr - much longer than the initial luminosity lifetime of 6-8 hr), the logarithm changes slowly and the integrated luminosity is proportional to the parameter τ_L. The initial luminosity lifetime $(dL/dt \ / \ L)^{-1}$ averaged over the first two hours of all Run II stores is presented in Fig. 6, and it shows a significant decline of the lifetime for higher luminosity stores. As we show later, beam-beam effects can reduce the luminosity lifetime by 10-15% and, thus, proportionally decrease the luminosity integral.

In summary, beam-beam effects in the Tevatron account for a 20-27% loss in the luminosity integral due to a) 10-12% particle loss before the start of collisions and b) 10-15% reduction in the luminosity lifetime. This loss is significant now, and it may be even larger after the luminosity upgrades, thus requiring continued systematic attention.

Our operational focus is to maximize integrated luminosity for the HEP program. Therefore, many studies presented in this paper were conducted

parasitically. The machine or beam parameters were rarely set to optimize specific beam-beam effects or to conduct a thorough, dedicated study. Instead, valuable information has been obtained by studying non-optimal settings for HEP runs or even unplanned incidents. Nevertheless, this paper presents observations and analysis valuable for future Tevatron operation.

2. HELICAL ORBITS

Beam-beam interactions differ between the injection and collision stages. The helical orbits should provide sufficient separation between the proton and antiproton beams in order to reduce detrimental beam-beam effects, e.g. tune shifts, coupling, and high-order resonance driving terms. Each bunch experiences 72 long-range interactions per revolution at injection, but at collision there are 70 long-range interactions and two head-on collisions per bunch. In total, there are 138 locations around the ring where beam-beam interactions occur. The sequence of 72 interactions out of the 138 possible ones differs for each bunch, hence the effects vary from bunch to bunch. The locations of these interactions and the beam separations change from injection to collision because of the antiproton cogging.

There are six separator groups (3 horizontal and 3 vertical) in the arcs between the two main interaction points, B0 (CDF) and D0. During collisions, these separators form closed 3-bumps in each plane, but the condition of orbit closure prevents running the separators at maximum voltages, thus limiting the separation at the nearest parasitic crossings 57 m away from the main IPs. To alleviate this limitation, additional separators can be installed in the arcs such that the separators form 4-bumps.

There is more flexibility in the helix design for the preceding stages: injection, ramp and squeeze. There are still some difficulties at these stages, including:

1) irregularities in betatron phase advance over the straight sections, especially A0;

2) aperture restrictions (physical as well as dynamic) that limit the helix amplitude at injection and at the beginning of the ramp;

3) the maximum separator gradient of 48 kV/cm (limited by separator spark rate) leads to a faster drop in separation $d \sim 1/E$ than in the beam size $\sigma \sim 1/E^{1/2}$ during the second part of the ramp above $E = 500$ GeV;

4) the polarity reversal of the horizontal separation during the squeeze (to satisfy needs of HEP experiments) that leads to a momentary collapse of the helix.

A simple figure of merit is helpful when comparing different helix designs. The conventional choice is the *minimum* value of the so-called *radial separation, S,* over all possible parasitic interaction crossing points in units of the RMS betatron beam sizes $\sigma_{x,y\beta}$:

$$S = \sqrt{(\Delta x / \sigma_{x\beta})^2 + (\Delta y / \sigma_{y\beta})^2} \ . \qquad (2)$$

The separation is normalized to a fixed reference emittance of 15 π mm mrad. Our experience has shown that less than 5-6σ separation causes unsatisfactory losses. Fig. 7 shows the minimum radial separation *S* during the ramp and squeeze with the initial helix design (blue, circa January 2002) and an improved helix (red, circa August 2004).

Early in 2002, the Tevatron luminosity progress was hampered by a very fast 20-35% loss of antiprotons occurring at sequence 13 of the low-beta squeeze. Figure 8 demonstrates how the initial luminosity actually decreased when attempting to bring higher intensity proton bunches to collisions. The luminosity decreased because of the larger antiproton losses at sequence 13. To solve this problem, the minimum separation was increased at that point from 1.8σ to 2.7σ by a) adding additional break points into the squeeze table, and b) tailoring the time dependence of separator voltages around the moment when the horizontal helix polarity changes. To minimize the total time spent in this dangerous condition, the time interval between the new break points was reduced from 5 sec to 2 sec. Any further time reduction is limited by the slew rate of the low-beta superconducting quadrupoles. Since implementing those changes, the antiproton losses in squeeze do not exceed 2-3%.

Beam separation at the injection energy was the subject of numerous improvements summarized in Table 2. The first two rows present the voltages on each separator plate used for antiproton injection, the corresponding values of minimum radial separation, the maximum absolute values of beam-beam tune shifts and resonance driving terms (RDTs) for $5\nu_x$ and $7\nu_y$ resonances over all antiproton bunches. The tune shifts were calculated for particles with small betatron amplitudes, whereas the RDTs give the increment in the action variable value for a resonant particle with an amplitude of 3σ in the corresponding plane. In the initial helix design, beam-beam effects were dominated by a single parasitic crossing near A0 (see Fig. 9). By employing two other separators (see Table 2), it was possible to reduce the RDTs and significantly increase separation at this point, while keeping it small at C0, the location of the smallest physical aperture at that time (mitigated in 2003). Together with the reduction in chromaticity from

8 to 4 units, which became possible in 2003 by introducing active transverse dampers and shielding the F0 Lambertson magnets with a conductive liner, the new helix significantly improved the antiproton lifetime at 150 GeV. It is possible to reduce beam-beam effects further at injection by using additional separators not presently powered at 150 GeV (see a "5*" helix in the third row of Table 2).

During acceleration, the separator voltages should increase as $E^{1/2}$ (E = beam energy) in order to maintain constant separation in units of the betatron beam size. Given the 48 kV/cm maximum operational gradient, the separators providing the bulk of the separation, B17H and C17V, reach their maximum voltage at $E \sim 500$ GeV. Above this energy, the radial separation drops as $1/E^{1/2}$ (Fig. 7). That leads to enhancement of detrimental beam-beam effects and causes particle losses. By employing additional separators (Table 2 bottom row), it was possible to increase the separation by more than 50% and to reduce beam losses above 500 GeV significantly. This improvement was achieved mainly by increasing vertical separation which was neither possible at injection, nor early on the ramp due to aperture limitations. The transition between the two types of helix, injection and end-of-ramp, manifests itself in Fig. 7 as a sharp maximum at 600 GeV. The new helix for the end of ramp and the first part of squeeze was introduced in August 2003.

The changes to the helix design, together with the reduction in chromaticity, drastically improved antiproton efficiency through injection, ramp and squeeze to well above 90% (see Fig. 3).

3. BEAM LOSSES DURING INJECTION AND ON RAMP

Although both the proton and antiproton beams stay at 150 GeV for less than an hour, a significant particle loss occurred during that time at the beginning of the Run II. As it will be shown below, the particle losses for both beams were driven by diffusion and exacerbated by small transverse and longitudinal apertures. The problem was alleviated significantly by a comprehensive realignment of many Tevatron elements in 2003-2004, as well as a reduction in the longitudinal emittances due to improvements in the Main Injector's bunch coalescing, and an increase of the Tevatron's dynamic aperture. Figure 10 presents the intensity lifetimes of single antiproton bunches after injection for typical stores in 2002 and 2004. It is clearly seen for both stores that the intensity decay is not exponential. Fig. 10 shows that the intensities are approximated well

by the expression $N(t) = N_0 e^{-\sqrt{t/\tau}}$ that was used for the lifetime fits. Similar $\sqrt{t}$ dependence has been observed for the bunch length shaving; Figure 11 shows an example of such behavior. The transverse emittances do not exhibit such dependence on $\sqrt{t}$.

Figure 12 shows, for many stores early in 2005, the antiproton bunch loss rate at 150 GeV as a function of the antiproton bunch emittance. One can see that the loss rate scales approximately as the square of the emittance. The data indicated by blue circles represents the same losses after reducing the chromaticity on the antiproton helix from *Q'=dQ/(dP/P)*=+(5-6) units to about 3. Although the functional dependence on the emittance is nearly identical, the absolute scale of the losses is reduced by a factor of ~5.

The example above demonstrates the importance of chromaticity for reducing the losses of both protons and antiprotons. Since the proton and antiproton orbits are separated using the electrostatic separators, their tunes and chromaticities can be controlled independently by using sextupole and octupole circuits, respectively. The major obstacle in attaining the desired chromaticity reduction was a weak head-tail instability in high intensity proton bunches [3]. Early in Run II, avoiding this instability required chromaticities as high as 8-12 units at 150 GeV. Reducing the proton chromaticities down to +(3-4) units became possible after removing unused high-impedance extraction Lambertson magnets, reducing the impedance of the injection Lambertson magnets by installing conductive liners, and commissioning active bunch-by-bunch instability dampers for the protons [4]. Decreasing the chromaticities to zero has become possible after reconfiguring octupole circuits to introduce Landau damping to suppress the head-tail instability. The antiproton bunches do not suffer from that instability since the intensity is much smaller than the protons. Consequently, both Q_x' and Q'_y are set closer to zero by using differential chromaticity octupole circuits.

During the roughly 20 minutes needed to load antiprotons into the Tevatron, the proton lifetime degrades as more antiproton bunches are injected (see Fig. 2). Figure 13 shows an approximately linear dependence of the proton loss rate at 150 GeV on the number of antiprotons in the Tevatron. The proton loss rate without antiprotons is about 4% per hour (25 hr lifetime), whereas it grows to about 16% per hour (6 hr lifetime) when all antiproton bunches are loaded. A similar linear dependence of the antiproton loss rate on proton intensity can be seen in the store-to-store antiproton inefficiency variations, but it can not be demonstrated as clearly as in Fig. 13, since the proton intensity at injection remains fairly constant over many months of operation.

Summarizing all of the above observations, one can parameterize the proton and antiproton intensity losses at 150 GeV that are driven by parasitic beam-beam interactions in the following relation:

$$\frac{\Delta N_{a,p}}{N_{a,p}} = 1 - \frac{N(t)}{N(t=0)} \propto \sqrt{t} \cdot \varepsilon_{a,p}^2 N_{p,a} Q'^2_{a,p} \cdot F(\varepsilon_L, Q_{x,y}, S_{a-p}) \tag{3}$$

where the index *a* or *p* stands for antiprotons or protons, ε is transverse emittance, *N* is total number of particles in the opposite beam, *Q'* is the chromaticity on the corresponding helix, and the factor *F* emphasizes the fact that losses also depend on the longitudinal emittance ε_L, separation *S* (size of the helix and cogging stage) and tune *Q*. Over years of operation, the betatron tunes on both helices at injection were optimized to be close to Q_x/Q_y = 20.584/20.576, i.e. above 7th order resonances at 4/7=0.5714, but close to the 12th order resonance 7/12=0.5833. Significant variations of the tune (in excess of ±0.002) often led to lifetime reduction, especially if the (vertical) tune approached the 4/7 resonance. Detailed work on optimization of beam-beam separation $S_{a\text{-}b}$ was presented in Section 2.

We believe that the observed $\sqrt{t}$ dependence of beam intensity decay and bunch length is driven by particle diffusion leading to particle loss at physical or dynamic apertures. The major diffusion mechanisms are intrabeam scattering (IBS), scattering on the residual gas, and diffusion caused by RF phase noise.

For example, if the available machine aperture is smaller than the beam size of the injected beam, the beam is clipped on the first turn with an instantaneous particle loss. Such a clipping creates a step-like discontinuity at the boundary of the beam distribution that causes very fast particle loss due to diffusion. The diffusion wave propagates inward, so that the effective distance is proportional to $\sqrt{t}$. Consequently, the particle loss is also proportional to $\sqrt{t}$. To estimate such a "worst-case loss", consider an initially uniform beam distribution: $f(I) = f_0 \equiv 1/I_0$, where I_0 is the action at the boundary. For sufficiently small time, $t << I_0 / D$, where *D* is diffusion coefficient, the diffusion can be considered one-dimensional in the vicinity of the beam boundary. Solving the diffusion equation

$$\frac{\partial f}{\partial t} = D \frac{\partial}{\partial I}\left(I \frac{\partial f}{\partial I} \right) \tag{4}$$

gives the result:

$$f(I,t) = \frac{2 f_0}{\sqrt{\pi}} \int_0^{(I_0 - I)/\sqrt{4 I_0 D t}} e^{-\xi^2} d\xi \ . \tag{5}$$

By integrating it over I, one obtains the dependence of particle population on time:

$$\frac{N(t)}{N_0} \approx 1 - \sqrt{\frac{t}{\tau}}, \quad \tau = \frac{\pi I_0}{4D}, \quad t << \tau \ . \tag{6}$$

In the transverse degree of freedom, the Tevatron acceptance at 150 GeV on the helical orbit is about $I^{tr}{}_0 \approx$ 50-80 π mm mrad, depending on the pre-shot machine tune-up, while the emittance growth rate is about $D^{tr} \approx$ 1-1.5 π mm mrad/hr chiefly from scattering on residual gas. So from (6), one can obtain a lifetime of τ≈30-80 hr. In addition, diffusion in the longitudinal plane with a rate $D^{long} \approx$ 0.03-0.3 rad^2/hr can lead to lifetimes of τ≈10-100 hr in the case where the longitudinal aperture is limited only by the RF bucket size $\sqrt{I_0{}^{long}} \approx 2$ rad. The above numbers are not well known, but we believe they are in the indicated ranges.

In reality, the machine acceptance is determined by the interplay between the physical and dynamic apertures. The latter is a strong function of the synchrotron action, and beam-beam interactions drastically reduce the dynamic aperture for synchrotron oscillation amplitudes close to the bucket size. Naturally, such an aperture reduction is stronger for larger values of chromaticity.

Several phenomena contribute to the losses observed during acceleration in the Tevatron. These include losses caused by shaving on a physical aperture, the limited dynamic aperture (DA) due to machine nonlinearities, the reduction of RF bucket area during the initial stages of the ramp, and beam-beam effects. Figure 14 shows the relative change of intensity during acceleration in store #3717 (August 2004). Most of the proton loss occurs during the first 10 seconds when the bucket area is decreasing [5]. Antiprotons are lost throughout the entire ramp, and until late 2004, the antiproton losses were much larger than proton losses. The time evolution of the antiproton losses is affected by the separator voltages. As it was explained above in Section 2, during the ramp these voltages increase linearly until about 500 GeV when the maximum voltage is reached. The beam separation, in units of the beam size, stays constant until 500 GeV but falls as 1/√E from 500 GeV to 980 GeV.

Dedicated studies were done in 2002-2003 to identify loss mechanisms that are unrelated to beam-beam effects. In several proton-only studies, protons with different intensities, transverse and longitudinal emittances were injected into the Tevatron and accelerated. These studies showed very clearly that the proton losses were determined by the longitudinal emittance and the longitudinal bunch profile. Short Gaussian bunches with bunch lengths < 2 ns at 150 GeV suffered the least losses ~2%, while long and non-Gaussian bunches suffered losses close to 10%. There was almost no dependence on the bunch intensity. Improvements in

bunch coalescing in the Main Injector have improved the beam quality significantly. In recent HEP stores (December 2004-April 2005), proton losses during acceleration are ~3% and are dominated by beam-beam effects – see Fig. 15.

Dedicated antiproton-only stores in 2002-2003 with showed that their losses without beam-beam effects were ~2%. However, during most of 2002 and 2003, antiproton losses during acceleration in stores were significantly higher at ~8-10%. Several accelerator chain improvements, extensive realignment and reshimming of dipoles in the Tevatron, and, more recently, using the Recycler to supply antiprotons to the Tevatron have resulted in significantly lower transverse antiproton emittances [2]. Changes were also made to the helix during the second half of the ramp, as described in a previous section. All of these changes have lowered the antiproton losses during acceleration to around 4-5% in recent stores (ca. April 2005). Figure 16 shows the dependence of antiproton losses during acceleration on the vertical emittance for two different stores. Store #3711 was a "mixed-source" store which included antiprotons from both the Accumulator and the Recycler, while store #3717 had only Accumulator antiprotons. Figure 16 displays several key features: 1) antiproton bunches from the Recycler have vertical emittances 4-5 π mm mrad smaller than those from the Accumulator, 2) there exists a clear correlation between the losses and the vertical, and 3) the antiproton losses are close to zero for vertical emittances below 6 π mm mrad. The losses do not correlate as strongly with the horizontal emittance, suggesting that the physical or dynamic aperture limitation on the antiproton helix is in the vertical plane. The antiproton losses up the ramp in the same two stores have almost no dependence on longitudinal emittance. In summary, combining observations presented in Figs. 15 and 16, beam losses on the ramp scale similarly to Eq. (3) as:

$$\frac{\Delta N_{a,p}}{N_{a,p}} \propto \varepsilon_{a,p}^2 N_{p,a} \cdot F_2(Q', Q_{x,y}, S_{a-p}) . \qquad (7)$$

Losses during the ramp are tolerable at present, but there is room for further improvements. Lowering chromaticities during the ramp with the help of octupoles will reduce proton losses that are mainly in the longitudinal plane. As antiproton intensities increase, beam-beam induced losses of protons during the acceleration may also increase. Smaller transverse proton emittances would help. Additional reductions in antiproton losses are possible with smaller antiproton transverse emittances, and that requires more bunches injected from the Recycler.

4. DIFFERENCES IN BUNCH-BY-BUNCH DYNAMICS

Remarkably, beam-beam effects in the Tevatron cause nearly every measurable indicator of beam dynamics to vary as a function of position within a bunch train. As mentioned above in Section 1, the 36 bunches for each beam are arranged in three trains of 12 bunches each, and the spread of intensities and emittances among the proton bunches is small. Consequently, a three-fold symmetry is expected [6] in the antiproton bunch dynamics. We have observed such behavior, so most of the plots below refer only to a single train of 12 bunches. For example, Fig. 17 shows that the helical orbits of antiproton bunches at 150 GeV and at low-beta differ by some 40 to 50 microns in a systematic, ladder-like fashion. Such variation in the closed orbits was predicted long ago [7], and agrees well with analytical calculations (see the comparisons in Fig. 17 (b) and (c)).

Two (vertical and horizontal) 1.7 GHz Schottky detectors [8] allow continuous, non-destructive measurements of betatron tunes and chromaticities for each proton and antiproton bunch during HEP stores. The tunes measured by the detectors represent an average over all particles in a bunch. The tune and chromaticity accuracies for single bunch measurements are better than 0.001 and 1 unit, respectively. A single measurement can be made in approximately 20 seconds.

Figure 18 presents the distribution of antiproton vertical and horizontal tunes along a bunch train. It is remarkable that bunches #1 and #12 have vertical and horizontal tunes, respectively, much lower (by more than 0.003) than the other ten bunches. Long-range beam-beam interactions at the parasitic IPs produce such significant bunch-by-bunch tune differences ΔQ_{LR}. The variation was expected before the start of Run II [6] and was studied experimentally in 1996 [9] using helical orbits somewhat different from what has been used in Run II. More detailed theoretically analyses are presented in [10, 11]. The data shown in Fig. 18 agree with analytic calculations if one takes into account that the measured tune is averaged over a weighted particle distribution, and, thus, the effective head-on tune shift is approximately half of the maximum beam-beam incoherent tune shift:

$$\Delta Q \approx \Delta Q_{LR} + 0.5 \cdot \xi, \quad \xi = \frac{r_p N_p}{4\pi(\varepsilon_p / 6)} \times 2, \tag{8}$$

where r_p denotes the classical proton radius, N_p is the bunch intensity, ε_p is the emittance, and the factor of 2 accounts for the two head-on interaction points. For

nominal bunch parameters at the beginning of an HEP store (see Table 1), the head-on tune shift for antiprotons is $\xi \approx 0.020$, while $\xi \approx 0.004$ for protons. Using the Schottky tune measurements, and taking (8) into account, the tune footprint of all proton and antiproton bunches at the beginning of a Tevatron store is plotted in Fig. 19.

The antiproton tunes decrease over the course of a store with characteristic decay times of 11-15 hr, caused by the reduction of the head-on tune shift, which itself is mostly due to the increase of proton emittances (by more than factor of 2) and the decrease of proton bunch intensities (by more than 25%). The time evolution of the measured antiproton tunes for two selected bunches in store #3678 is shown on Fig. 20.

Within the accuracy of the detectors, the proton tunes are identical for all bunches, and are usually stable over duration of HEP stores (16-30 hours). Small, but noticeable, decreases of both vertical and horizontal tunes by ≈(0.0005-0.001) over the first few hours agree with the expected decrease of the head-on tune shifts for protons.

The chromaticity measured by the same system is remarkably stable within 1 unit during the store. Since no time dependence is observed, averaging the data over the entire store seems fair. Even so, the chromaticity does depend on the bunch number within a train, as shown in Fig. 21. Chromaticity varies by about 6 units in both planes along a bunch train, and that is in acceptable agreement with theory that considers both parasitic beam-beam interactions, as in [11] (which predicts the variation to be significant only in horizontal plane), and the energy-dependence of the beta functions at the main IPs.

It is not surprising that with such significant differences in orbits, tunes and chromaticities, the antiproton bunch intensity lifetime and emittance growth rates vary considerably from bunch to bunch. For example, Fig. 22 presents the beam-beam induced intensity loss rates for antiproton bunches observed in the first two hours of 20 HEP stores during summer 2004. To calculate such a loss rate, called the non-luminous (NL) loss rate, one subtracts the particle losses due to collisions at the main IPs $d\ln N/dt = L\sigma_{tot}/N$ (luminosity L is measured bunch-by-bunch by both detectors, $\sigma_{tot} \approx 70$ mb at the Tevatron center-of-mass collision energy [12]) from the total measured bunch intensity loss rate $d\ln N/dt$. The error bars represent the RMS store-to-store fluctuations in the loss rates. One can see that bunch #1 systematically loses less intensity than the others (of about 0.3% per hour or 300 hours of lifetime), while bunches #4 and #12 lose more than 1% per hour (i.e. their NL lifetime is 70-90 hours). In comparison, the average luminous antiproton loss rate $d\ln N/dt = L\sigma_{tot}/N$ is about 3%/hr or 30 hours of lifetime for a typical high luminosity store. Thus, beam-beam effects account for, on average, up to ≈15% of

the antiproton loss rate (and ≈30% for bunches #4 and #12). Later in stores, the luminous losses decrease faster than NL losses, and the two often become comparable or the NL losses can even dominate. Other mechanisms of NL beam loss, like collisions with residual gas and losses from the RF buckets, are much weaker than beam-beam effects, and they account for less than 0.1%/hr of the intensity loss.

Experiencing the largest beam-beam tune shift in any hadron collider, antiproton bunches in the Tevatron may suffer emittance growth as a result of strong higher order resonances if the working tune point is not optimized. As with the significant bunch-by-bunch tune variations, this growth can be quite different for different bunches in the bunch train. As an illustration, Fig. 23 (a) presents the time evolution of the vertical emittance of bunches #1, 6, 11, 12 after collisions began in store #3554 (June 2, 2004) . One can see that within 10-15 minutes, some bunches experience 10-20% transverse emittance blowup that reduces collider luminosity. Figure 23 (b) summarizes the total emittance blowup in that store for one train of antiproton bunches. One can see a remarkable distribution along the bunch train which gave rise to term "scallops" (three "scallops" in three trains of 12 bunches) for this phenomenon – the end bunches of each train have lower emittance growth than the bunches in the middle of the train. The scallops depend strongly on the machine working point (vertical and horizontal tunes) since the tune shift for a given bunch depends on its position within a train. Figure 24 shows a two-dimensional contour plot of the maximum (over all antiproton bunches) emittance blowup vs the average antiproton vertical and horizontal tunes measured by the 1.7 GHz Schottky detectors in the first few minutes of all HEP stores in 2004. Taking into account Eq. (7), one can conclude that the vertical emittance blowup is strongest when the core particle vertical tune approaches either the 5^{th} order resonance or the 12^{th} order resonance Q_y=7/12=0.583. In the horizontal plane, the scallops are small if tune is set away from Q_x=3/5=0.600. Scallops were first observed in 2003, when the head-on tune shift parameter increased to 0.02. Various methods have been employed to minimize the development of scallops (including a successful attempt to compensate one bunch emittance growth with a Tevatron Electron Lens [2, 13]), but carefully optimizing the machine tunes was found to be the most effective. As one can understand from Fig. 19, one should balance between the desire to lower the core antiproton tunes away from $3/5^{th}$ resonance and the fact that halo antiprotons are lost more quickly when their tunes are on $7/12^{th}$ resonances.

Much smaller "scallops" of ~0.5 π mm mrad were observed infrequently in proton bunches when their tunes were set near 12^{th} order resonances, but they were corrected easily by tune adjustments and have not been as serious an issue as the antiproton emittance growth.

Another interesting beam-beam related phenomenon happens to the proton beam. It was originally observed in the Fall of 2003 that the proton halo count rates in the CDF detector follow the proton intensity loss rates that vary significantly by a factor of 4-6, in a systematic fashion, along a bunch train as seen in Fig. 25: the losses were lower for bunches at the start of each train and larger near the end of each train. We identified the source of this behavior as the transverse size mismatch for head-on collisions of larger emittance proton bunches with smaller emittance antiproton bunches; this phenomenon has been observed in other accelerators [14]. As shown in Fig. 3 (c), antiproton bunches at the beginning of the trains have emittances more similar to the protons than do the antiprotons at the end of trains. Figures 26 and 27 present statistics of the proton NL loss rates for all 36 bunches in 51 HEP stores in Dec. 2004-Mar. 2005 which can be can be summarized as:

$$\frac{1}{\tau_p} = \frac{1}{N_p}\frac{dN_p}{dt} \propto \frac{N_a}{\varepsilon_a^2} \cdot F_3(Q_{x,y}, Q', \varepsilon_p) \qquad (9).$$

Error bars representing RMS fluctuations from store to store demonstrate the volatility of the losses. It is noteworthy that proton NL loss rates are often much higher than the intensity decay rate due to luminosity, which is of the order of 0.2-0.3%/hr for typical initial luminosities, and higher than antiproton NL loss rates - compare the vertical scales in Figs. 22, 26 and 27. The NL proton losses are also much higher than losses due to collisions with residual gas and losses out of the RF buckets, both of which are less than 0.1%/hr. The volatility and scale of the NL proton losses are of concern for the detectors since high halo rates deteriorate their data-taking efficiency and, in general, they reduce the luminosity lifetime and the integrated luminosity per store. Again, the most effective way to control the losses has been to adjust the working point. In particular, it was found that the losses were much higher when the proton tunes lay over the 12^{th} order resonance lines, and Fig. 25 shows that proton lifetime there was only 25-30 hours on average. After the proton tunes were moved below the 12^{th} order resonances (as shown in Fig. 19), the lifetime improved.

5. OTHER EXPERIMENTAL OBSERVATIONS

The two types of the beam-beam effects in the Tevatron, long-range and head-on, have quite different manifestations. In general, the long-range effects should depend on a) beam separation, b) transverse emittances of beams; c) total intensity in opposite beam; d) momentum spread; e) lattice parameters like tunes, chromaticities and coupling; f) available beam aperture; g) cogging and bunch position in the bunch train. In contrast, head-on collision effects should be

affected by a) bunch intensity in opposite beam; b) transverse emittance of the opposite bunch; d) tunes, chromaticities and coupling. It is obvious that at injection and on the ramp, only the long-range interactions matter since the beams are separated everywhere around the ring. After the head-on collisions are initiated, the ratio between the two types of interactions can be observed in the following examples.

First, Fig. 28 shows non-luminous proton losses during store #4111 (April 24, 2005), in which only 24 antiproton bunches were loaded instead of the usual 36 due to problems in the injector chain. As a result, proton bunches #9-12 did not collide "head-on" with any antiproton bunches at the IPs, but experienced most of the possible long-range interactions (except for some of the parasitic collision points nearest to the IPs). The measured intensity loss for those particular proton bunches were extremely small: 0.03-0.06 %/hr. That rate is consistent with the 1000-2000 hr lifetime expected solely from beam-gas interactions. One can conclude that the long range beam-beam interactions with antiprotons do not affect proton bunch lifetime. The other bunches shown in Fig. 28 were colliding head-on with various antiproton bunches of various emittances, and their pattern of the rates follows Eq. (9).

Figure 29 presents both proton and antiproton losses at the beginning of another unfortunate store #3869 (Dec 20, 2004) when, due to a hardware malfunction, the voltage on one of two plates of B11 horizontal separator was set to 15 kV instead of desired 98 kV. As a result, the beams were separated at both IPs by about 90 μm (2.6 σ) that caused a factor of 5.5 reduction of luminosity. In addition, horizontal separation at a parasitic interaction point close to the D0 IP was reduced from 0.62 mm to 0.34 mm. The voltage problem was fixed in about 20 min, and the luminosity went up to 45 10^{30} $cm^{-2}s^{-1}$, as expected for the given intensities and emittances. During the 20 min with the incorrect separator voltage, both proton and antiproton intensity lifetimes were very short (~16-20 hr) and dominated by non-luminous losses. The distribution of these losses along the bunch train was quite different for protons and antiprotons (see Fig. 29). The antiproton losses varied by factor >10 from bunch to bunch, reaching a maximum for the bunches at the ends of the three trains (#12, #24, #36) – as expected if antiprotons were affected mainly by parasitic collision points near the main IPs. The proton losses went up in a much more uniform manner, with a small variation due to differences in the opposing antiproton bunch emittances (similar to Fig. 25).

Figure 30 shows the antiproton non-luminous loss rate dependence on the helix size in about 35 HEP stores in March-April 2005. In each of these stores, voltages of all 24 separators were scaled from their nominal values either by

+10% (11 stores) or by -10% (6 stores) or set nominal (18 stores). The voltages stayed the same for the entire length of store, and the voltages were changed only on a store-to-store basis. The typical initial luminosities were similar for all three sets (from 80 10^{30} cm^{-2} s^{-1} to 115 10^{30} cm^{-2} s^{-1}). There was no systematic variation in proton non-luminous lifetime for these stores. In contrast, the non-luminous antiproton loss rates decreased as the helix size *S* increased approximately as $1/S^3$: they varied by ±30% for -+10% variation of the helix size.

All three facts presented above point to two conclusions: a) the main adverse effect on antiprotons during HEP comes from long-range interactions, especially at the nearest parasitic interaction points; b) head-on collisions dominate proton losses. Both conclusions are expected for the situation when a larger emittance, high intensity proton beam collides with a lower intensity (factor of 5 to 9), smaller emittance (factor of 1.2-2.5) antiproton beam.

The proton and antiproton dynamics also differ in the evolution of their longitudinal distribution functions during HEP stores. Figure 31 shows that at the beginning of the store #3678 (July 2004), both proton and antiproton distributions are contained within 5.0 eV sec. For protons, diffusion due to IBS and RF phase noise over 34 hours led to an increase of both the average action and tails beyond 5.0 eV sec. For antiprotons, there is no tail seen in the final distribution, although the average action clearly increased. The antiprotons with large synchrotron amplitudes have a higher transverse diffusion rate due to multiple crossings of higher-order beam-beam resonances, consequently they have shorter lifetime.

One can summarize all data on antiproton intensity lifetime in collisions presented in this and previous chapters as following:

$$\frac{1}{\tau_a} = \frac{dN_a}{N_a dt} \propto N_p \frac{\varepsilon_a^2}{S^3} \cdot F_4(Q_{x,y}, Q', M, \varepsilon_L), \qquad (10)$$

where *M* stands for bunch position in bunch train, ε_L is the longitudinal emittance.

All beam-beam effects observed in the Tevatron depend strongly on particle tunes or working points (WPs). Dedicated experiments to explore these effects have not been conducted because that would require wasting antiprotons needed for HEP - the scans can be quite detrimental and lifetime can deteriorate significantly. Instead, proton and antiproton tunes at injection energy and in collisions have been changed only slightly and not very often over periods of weeks or months. Most operational efforts were focused on keeping machine WPs as close as possible to the "golden ones" (those where machine performance is the best or most reliable). As mentioned previously, deviation of the beam tunes from those optimal values by few 0.001 usually resulted in significant changes (typically deterioration) of Tevatron efficiencies and/or lifetimes. Nevertheless,

at the end of HEP stores, when luminosity is many times smaller than the peak, the experiments are more willing to sacrifice a few hours of integrated luminosity and to accept higher than usual background radiation rates. They usually turn off power to the most critical systems, like silicon vertex detectors, and only leave on the instrumentation needed for the accelerator physics experiments, such as luminosity counters and halo monitors. During studies in which beam position is changed, these counters correctly reflect variations of corresponding beam lifetimes. Since these counters are very sensitive to losses and have large bandwidth (report data at least once a second), they can be used for fast WP scans near the optimal working points. Existing beam diagnostics provide bunched beam intensity measurements with a precision of 0.2-0.6%, so significant time would be needed to determine beam lifetime if it exceeds 10 hours. The use of the detector halo rate counters is limited by their maximum counting rates – counters usually saturate if the lifetime drops below 1-2 hours. The contour plots presented in Fig. 32 show variations of the proton and antiproton halo rates during WP scan at the end of store #3972 on February 10, 2005. The beams were quite diffuse by this time, so the antiproton head-on tune shift Eq. (8) was only about 0.007, and the proton tune shift was about 0.001 (many times smaller than at the start of the store). The proton and antiproton tunes were measured by the 1.7 GHz Schottky tune meter. The tunes were changed simultaneously over a wide range in steps of 0.001. One can see a significant loss rate enhancement for protons at Q_x=.571 and Q_x=.571 (near 7th order resonance), a detectable increase at Q_x/Q_y=.583/.583 (12th order resonance), and when the tunes approached the strong 5th order resonance $Q_x/Q_y \rightarrow$.600. Antiproton loss rates went up in the vicinity of 12th and 5th order resonances as well. From these scans, one can conclude the best working points are at Q_x/Q_y=.593/.588 for antiprotons and Q_x/Q_y=.590/.590 for protons. The beam lifetimes at those tunes were about 100-160 hours for both beams. Similar results were obtained in another WP scan at the end of store #2072 (Dec 14, 2002) [15].

6. DISCUSSION AND CONCLUSIONS

As mentioned in the introduction, the luminosity integral $I=\int L dt$ – the sole critical parameter for HEP experiments – depends on the product of peak luminosity and the luminosity lifetime, e.g. for a single store with initial luminosity L_0 and duration T, the integral is $I \approx L_0 \tau_L \ln(1+ T/\tau_L)$. The initial luminosity can be obtained from a well-known formula for luminosity in head-on collisions

$$L = \gamma f_B \frac{N_a N_p}{4\pi\beta^*(\varepsilon/6)} H(\sigma_s/\beta^*), \qquad (11)$$

where ε is the average 95% normalized emittances of two round beams $(\varepsilon_a+\varepsilon_p)/2$, *H(x)* is the "hourglass factor" which depends on the ratio of the RMS bunch length σ_s and beta-function at IPs β^*, γ is the relativistic factor, and f_B is the frequency of bunch collisions. Beam losses at 150 GeV and up the energy ramp are mostly due to beam–beam interactions. They are accompanied by small longitudinal emittance reduction, but they do not result in significant changes of transverse emittance. Presently, these losses account for a total of 3-9% at 150 GeV and 6-10% on the ramp. What is remarkable is that the fractional losses of the "strong" (higher intensity) proton beam are of the same order, or sometimes even exceed, the losses from the weak antiproton beam. Equation (3) explains that phenomenon: indeed, the proton intensity is 6-9 times higher and the transverse emittance of protons is some 50% larger, but the chromaticity on the proton helix has to be held two or more times higher than on the antiproton helix in order to control the head-tail instability. In any event, the root cause for both proton and antiproton losses are parasitic long-range beam-beam interactions.

Rapid antiproton emittance growth after initiating head-on collisions ("scallops") of the order of 2 π mm mrad led to a peak luminosity reduction $dL/L \sim - d\varepsilon_a/(\varepsilon_a+\varepsilon_p)$ of about 6% until a better working point was implemented.

From Eq.(11), the luminosity lifetime has four constituents:

$$\tau_L^{-1} = \frac{dL(t)}{L(t)dt} = \mid \tau_\varepsilon^{-1} \mid + \tau_{Na}^{-1} + \tau_{Np}^{-1} + \tau_H^{-1} . \qquad (12)$$

For 2004-2005 Tevatron collider operation with range of initial luminosities between 0.6 and 1.2 10^{32} $cm^{-2}s^{-1}$, the largest contribution to luminosity decay came from beam emittance growth with a typical time of $\tau_\varepsilon \sim$ 15-20 hr. The growth is dominated by intrabeam scattering (IBS) in the proton bunches, with small contributions from the IBS in antiprotons and external noises. Beam-beam effects, if noticeable, usually manifest themselves in reduction of the beam emittances or their growth rates rather than in increases. The antiproton bunch intensity lifetime $\tau_a \sim$ 20-25 hours is dominated by the luminosity burn rate which accounts for 80-90% of the lifetime, while the remaining 10-20% comes from parasitic beam-beam interactions with protons. Proton intensity loss is driven mostly by head-on beam-beam interactions with smaller size antiprotons at the main IPs, and varies in a wide range $\tau_p \sim$ 35-200 hr. The proton lifetime caused by inelastic interactions with antiprotons in collisions and with residual gas molecules varies from 200 to 400 hours. The hourglass factor decays with $\tau_H \sim$ 70-80 hours due to the IBS, again, mostly in proton bunches. Beam-beam effects may lead to reduction of the proton bunch length growth (longitudinal "shaving") in a poorly tuned machine. Antiproton bunch lengthening slows down later in the

store when approaching a dynamic aperture due to beam-beam effects, as was shown in Section 5. Combining all of these loss rates together as in Eq. (12), one gets the observed initial luminosity lifetime (averaged over the first two hours of store) of about $\tau_L \sim 7.5$-9 hours, as shown in Fig. 5. At present operational conditions (Spring 2005), beam-beam effects reduce luminosity lifetime by 10-15%.

The goal of the Run II luminosity upgrade project is to attain three times more antiprotons delivered to collisions in the Tevatron by improving the antiproton production rate in the source [2]. The parameters of proton bunches are not expected to differ much from present values, while antiproton transverse emittances may be up to 50% larger than the present (see Table 1). By applying the scaling laws from Eqs (3), (7), (9) and (10), one expects the total beam losses preceding collisions (at injection and on the ramp) will increase from 19% now to about 42%, while the luminosity lifetime will be reduced a similar 10-15% (though the lifetime itself will be significantly smaller). Even if the emittances of antiprotons cooled in the Recycler ring will be the same as for present operations, the inefficiency before the collisions still will be about 30%. Note, that according to the same scaling laws, increasing the proton bunch intensity by 25% should not change the beam-beam inefficiencies drastically (increase the antiproton losses 2-3%) if the proton emittances would remain the same.

The numbers for the Upgrade parameters do not look very optimistic, so we plan to continue to counteract the adverse beam-beam effects. The planned measures include: a) increasing beam separation on the ramp and in collisions by using additional separators or higher voltage separators; b) reducing chromaticity on the ramp and in collisions by the possible use of octupoles or by employing transverse instability dampers; c) moving the proton WP above the 7/12 resonance; d) stabilizing the antiproton and proton tunes during HEP stores; e) reduce antiproton and proton emittances; f) compensating beam-beam tune shifts with electron lenses; g) betatron phase adjustment between two IPs.

This article is the most systematic presentation to date of beam-beam phenomena in the Tevatron and the results of relevant beam studies. We have shown that beam-beam effects dominate beam losses at the 150 GeV injection energy and on the ramp, and significantly reduce beam lifetime during collisions. Antiproton losses at all stages of the Tevatron stores are caused by long-range interactions with protons. Proton losses before collisions are also due to long-range effects, while the proton lifetime reduction in collisions is mostly due to head-on interactions with smaller size antiproton bunches. Currently, various beam-beam effects reduce the integrated luminosity by 20-25%. Several scaling laws were derived to summarize beam-beam observations in the Tevatron. They

predict that after anticipated upgrades of the antiproton production complex and a three-fold increase of antiproton intensity, the beam-beam effects can reduce the luminosity integral by as much as 40-50% if not counteracted. Therefore, the work on understanding and mitigation of the beam-beam effects will continue.

We would like to thank A.Xiao, P.Ivanov, J.Annala, T.Bolshakov, A.Jansson, R.Pasquinelli, C.Y.Tan, R.Flora, S.Pordes, J.Marriner, M.Xiao, B.Erdelyi, E.McCrory, D.McGinnis, J.Morgan, J.Steimel (FNAL) and F.Zimmermann (CERN) for valuable input, assistance during beam studies and useful discussions on the subject.

7. REFERENCES

[1] Tevatron Run II Handbook, http://www-bd.fnal.gov/runII.
[2] V.Shiltsev, in Proc. EPAC 2004 (Lucern), p. 239.
[3] P.Ivanov, *et al.*, in Proc. IEEE PAC 2003 (Portland), p. 3062.
[4] C.Y.Tan, J.Steimel, in Proc. IEEE PAC 2003 (Portland), p. 3074.
[5] T.Sen, *et al.*, in Proc. IEEE PAC 2003 (Portland), p. 1754.
[6] P.Bagley, *et al.*, FNAL Preprint Conf-96-392 (1996).
[7] L.Michelotti, FNAL Preprint TM-1738 (1995).
[8] R.Pasquinelli, *et al.*, in Proc. IEEE PAC 2003 (Portland), p. 3068.
[9] P.Bagley, in Proc. EPAC 1996 (Barcelona), p. 1155.
[10] Yu.Alexahin, FNAL Preprint Pub-00-120-T (2000).
[11] T.Sen, *et al.*, Phys. Rev. ST Accel. Beams **7**, 0410101 (2004)
[12] S. Eidelman *et al*., Phys. Lett. B**592**, 1 (2004), p. 4011.
[13] V.Shiltsev, *et al*, Proc. HALO'03, AIP Conf. Proc. **693** (2004), p. 256.
[14] K.Cornelis, in Proc. LHCBB '99 (Geneva), CERN-SL-99-039-AP, p. 2.
[15] X.Zhang, *et al.*, in Proc. IEEE PAC 2003 (Portland), p. 1757.

TABLE I. Tevatron collider parameter list.

Parameter	Present	Upgrade	Units
Peak luminosity	1.2	2.7	10^{32} cm^{-2} s^{-1}
Integrated luminosity	21	47	pb^{-1}/wk
Total delivered $\int L\,dt$	1.1	4.4-8.8	fb^{-1}
Beam Energy	980	980	GeV
Number of bunches	36x36	36x36	
Bunch spacing	396	396	ns
Protons/bunch	260	270	10^9
Antiprotons/bunch	43	127	10^9
Proton emittance, 95%	19	20	π mm mrad
Antiproton emittance, 95%	14	20	π mm mrad
β^* at IP	35	35	cm
Hourglass factor	0.65	0.65	
Max antiproton production rate	16	45	10^{10}/hr

TABLE II. Electrostatic separator power supply voltages, minimum beam-beam separations S for a reference emittance of 15 π mm mrad, tune shifts and resonant driving terms of $5\nu_x$ and $7\nu_y$ resonances (RDT). Positive voltages correspond to horizontally outward and vertically upward kicks for protons. The tune shifts were calculated for particles with small betatron amplitudes. The RDTs are calculated for the design proton intensity of $2.7\cdot10^{11}$/bunch. The RDTs give the increment in the action variable value for a resonance particle with an amplitude of 3σ in the corresponding plane. The tune shifts and RDTs presented here are the maximum absolute values for all antiproton bunches.

Helix	Separator Power Supply Voltage (kV)					S_{min}	Tune shifts		RDTs (m/turn)	
	B11H	B17H	B11V	C17V	C49V		$\lvert\Delta Q_x\rvert$	$\lvert\Delta Q_y\rvert$	$\lvert R_{50}\rvert\cdot10^{11}$	$\lvert R_{07}\rvert\cdot10^{13}$
Jan 2002	0	61.7	0	-61.7	0	4.83	.0045	.0020	1.95	7.06
May 2002	-37	64.3	-22.6	-58.8	0	6.01	.0028	.0019	0.92	1.77
"5 star"	-18.9	61.8	5.9	-68.4	21.8	7.34	.0020	.0009	0.80	0.55
End of Ramp	0	118.9	-21.0	-118.9	62.6	5.08	.0033	.0016	0.67	1.95

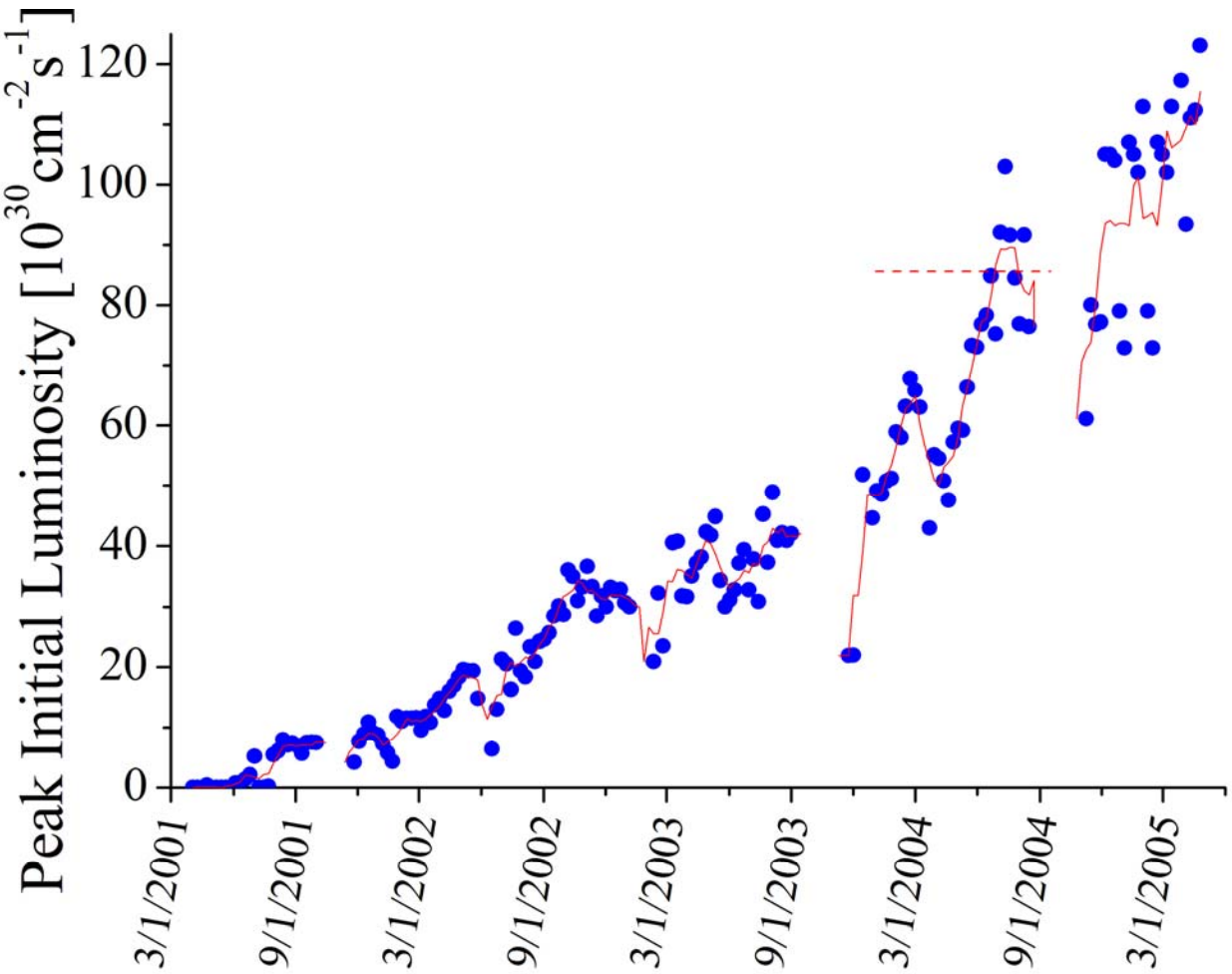

FIG. 1. Tevatron luminosity progress in 2001-2005. Each dot represents a weekly maximum initial peak luminosity averaged between CDF and D0 detectors. The solid red line is a running four-week average. The dashed red line at L=0.86 10^{32} $cm^{-2}s^{-1}$ the initial Run II peak luminosity goal without electron cooling in the Recycler ring [1].

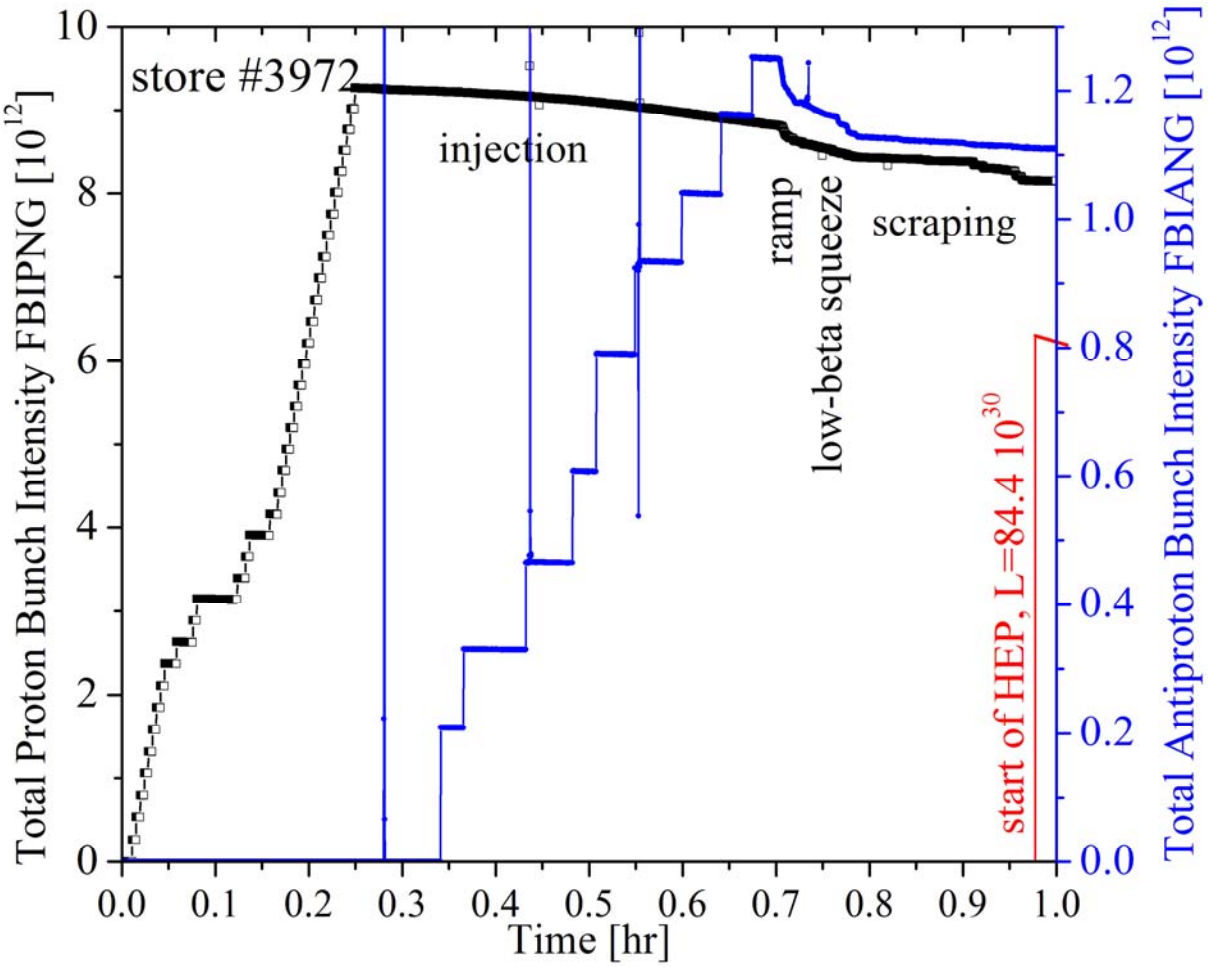

FIG. 2. Injection process and beginning of the luminosity run in store #3972 (February 8, 2005). The black and blue dots are the total proton and antiproton bunch intensities, respectively (measured by a Fast Bunch Integrator system). The red line represents the start of the HEP store with an initial peak luminosity of 84.4 10^{30} cm^{-2} s^{-1}. Major steps in the process are marked. The four spikes in the antiproton intensity are artifacts of the Fast Bunch Integrator that occur when proton bunches pass antiproton bunch integration gates during the longitudinal cogging.

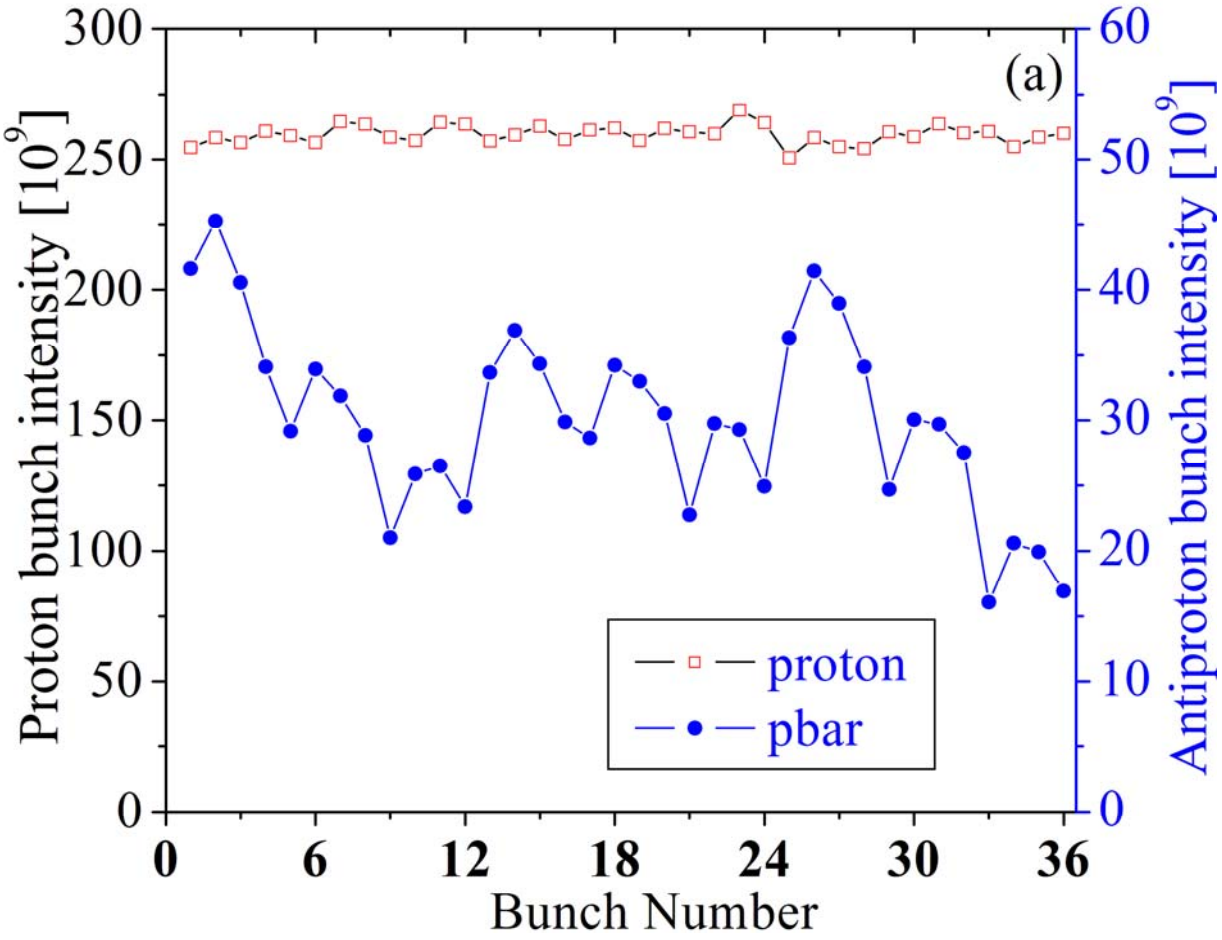
(a)
Proton bunch intensity [10^9]
Antiproton bunch intensity [10^9]
Bunch Number
proton
pbar
0
50
100
150
200
250
300
0
10
20
30
40
50
60
0
6
12
18
24
30
36

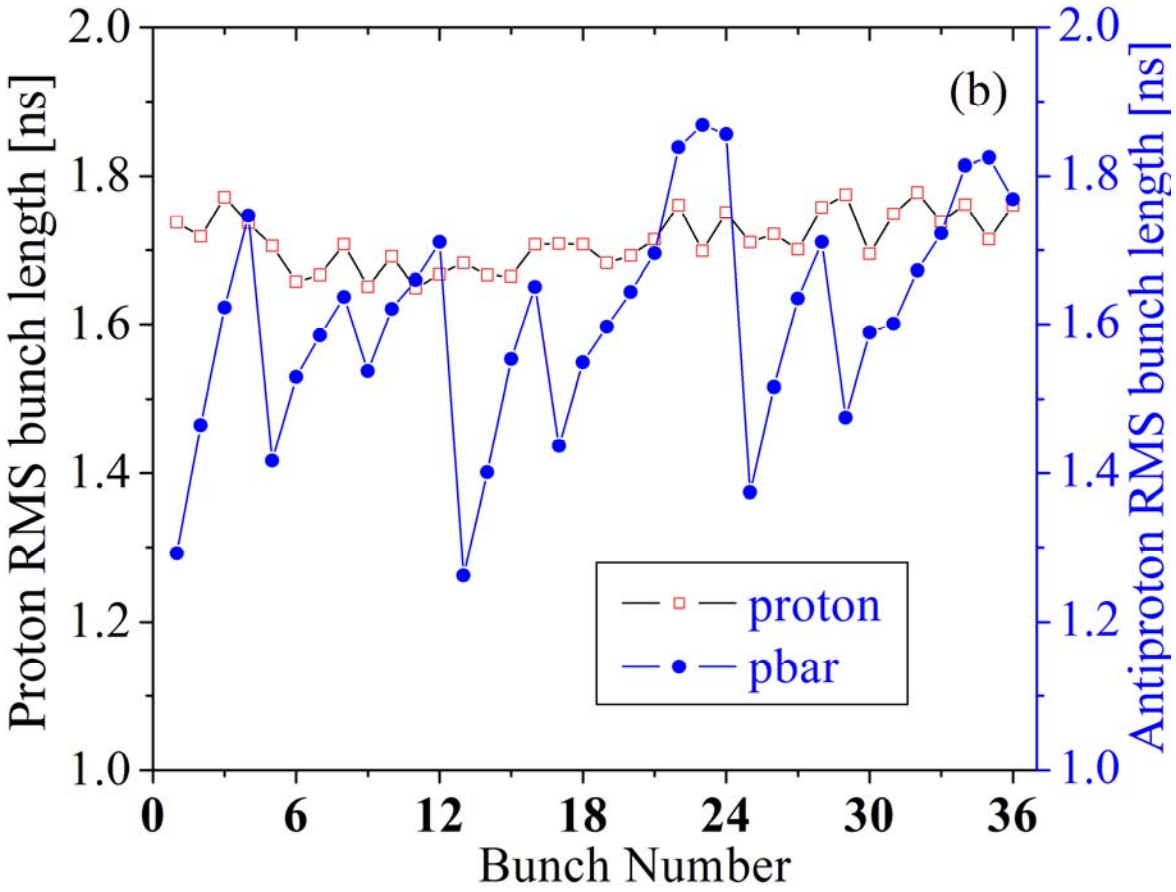
(b)
Proton RMS bunch length [ns]
Antiproton RMS bunch length [ns]
Bunch Number
proton
pbar
2.0
1.8
1.6
1.4
1.2
1.0
0
6
12
18
24
30
36

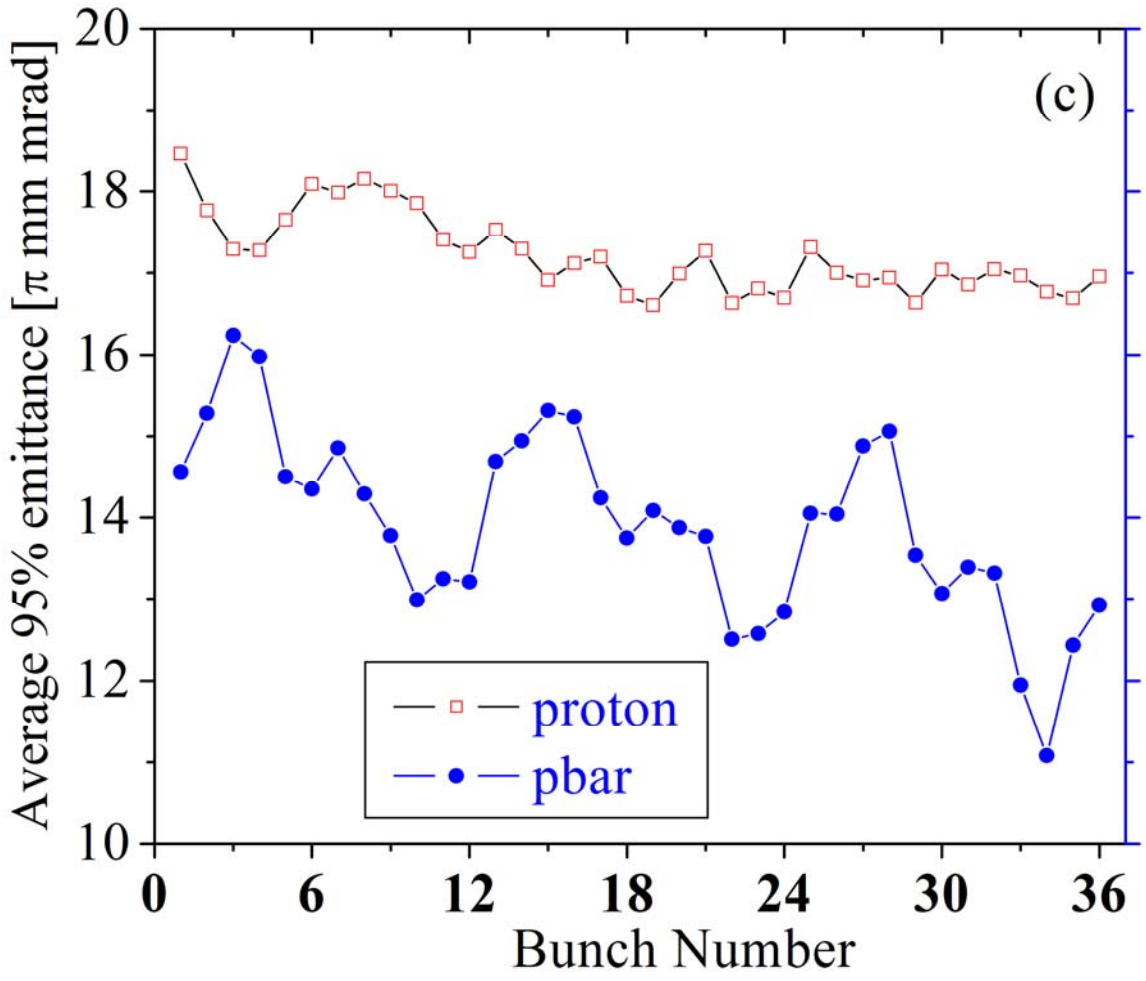

FIG. 3. Distribution of (a) proton and antiproton bunch intensities, (b) RMS bunch lengths , and (c) average (vertical and horizontal) emittances at the start of HEP store #3692 (July 31, 2004). All of the variations are caused by the injectors, except for a small increase in the emittance of the first two proton bunches due to an injection kicker imperfection.

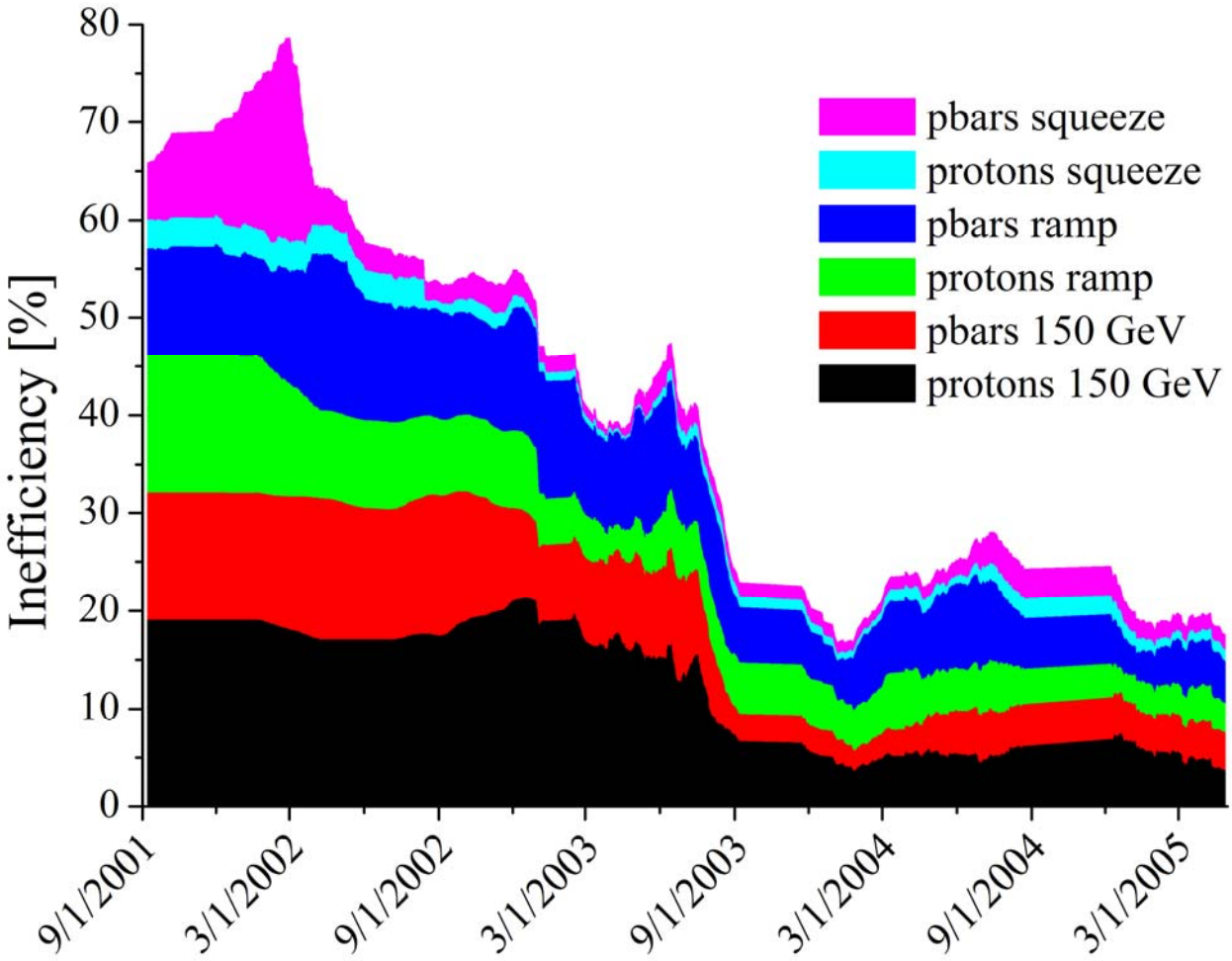

FIG. 4. Chart of the Tevatron beam inefficiencies at various stages. The inefficiency is a ratio of the total bunched beam intensity lost during a stage to the intensity at the start of a stage. The running averages over 20 stores are presented.

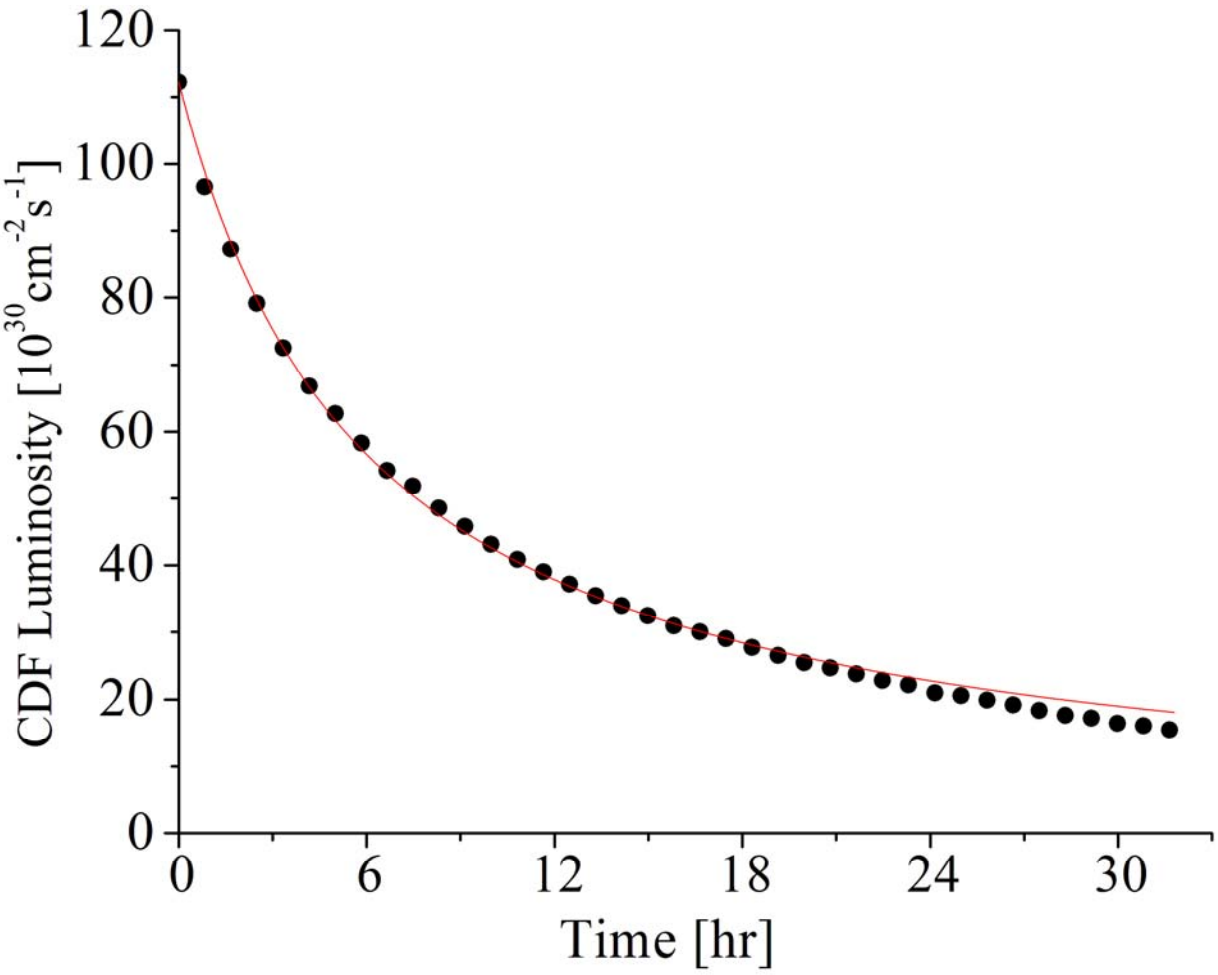

FIG. 5. Evolution of instantaneous luminosity at the CDF detector in store #3657 (July 16, 2004). The blue dots are the CDF luminosity measurements, and the red line is the fit to Eq. (1) with the ½ -decay time of τ_L=6.1 hr.

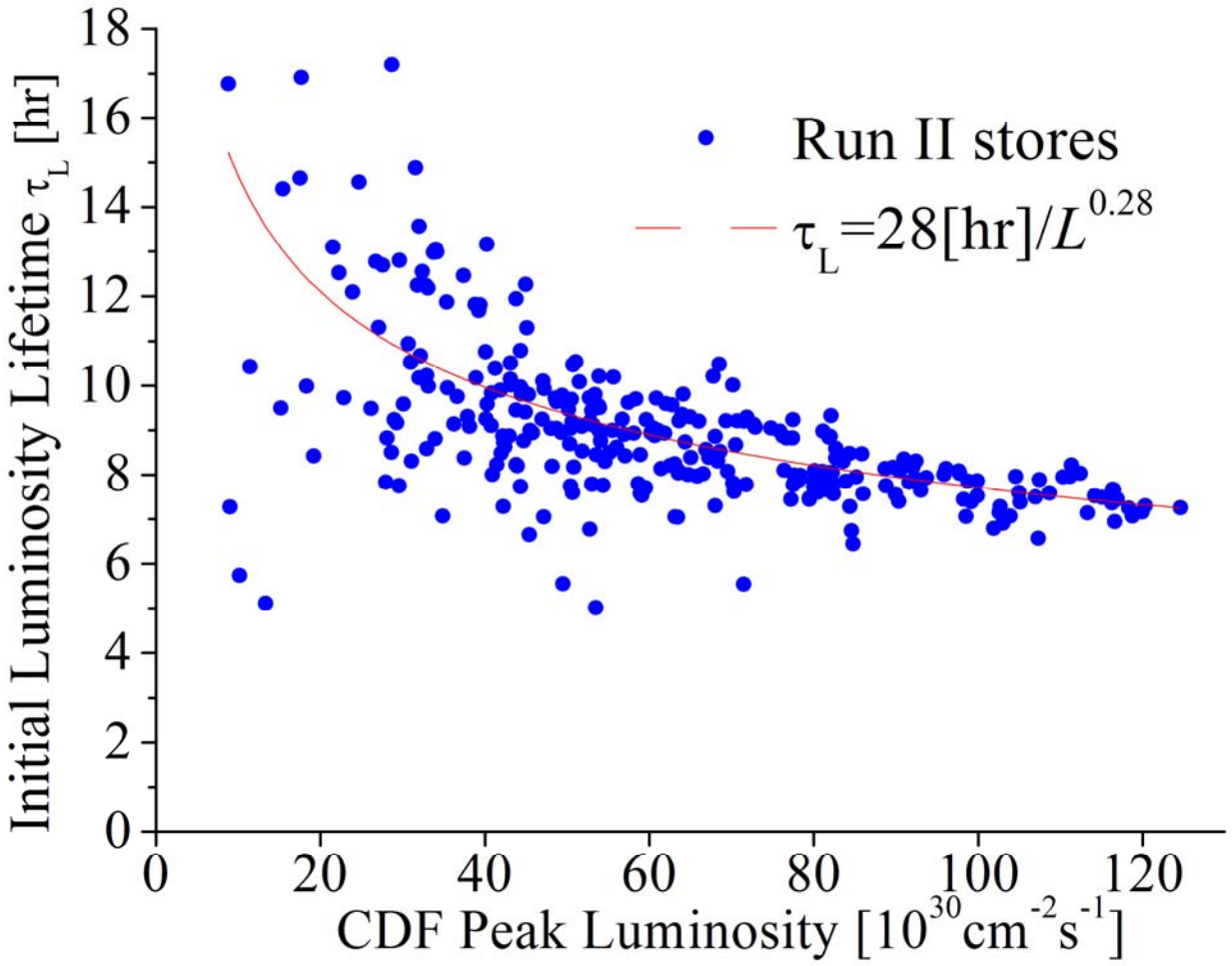

FIG. 6. Luminosity lifetime averaged over the first two hours of all HEP stores vs the initial CDF luminosity. The blue dots are the data , and the red line represents a fit of the data to the function $\tau_L(L)=28\ \mathrm{hr}/L^{0.28}$.

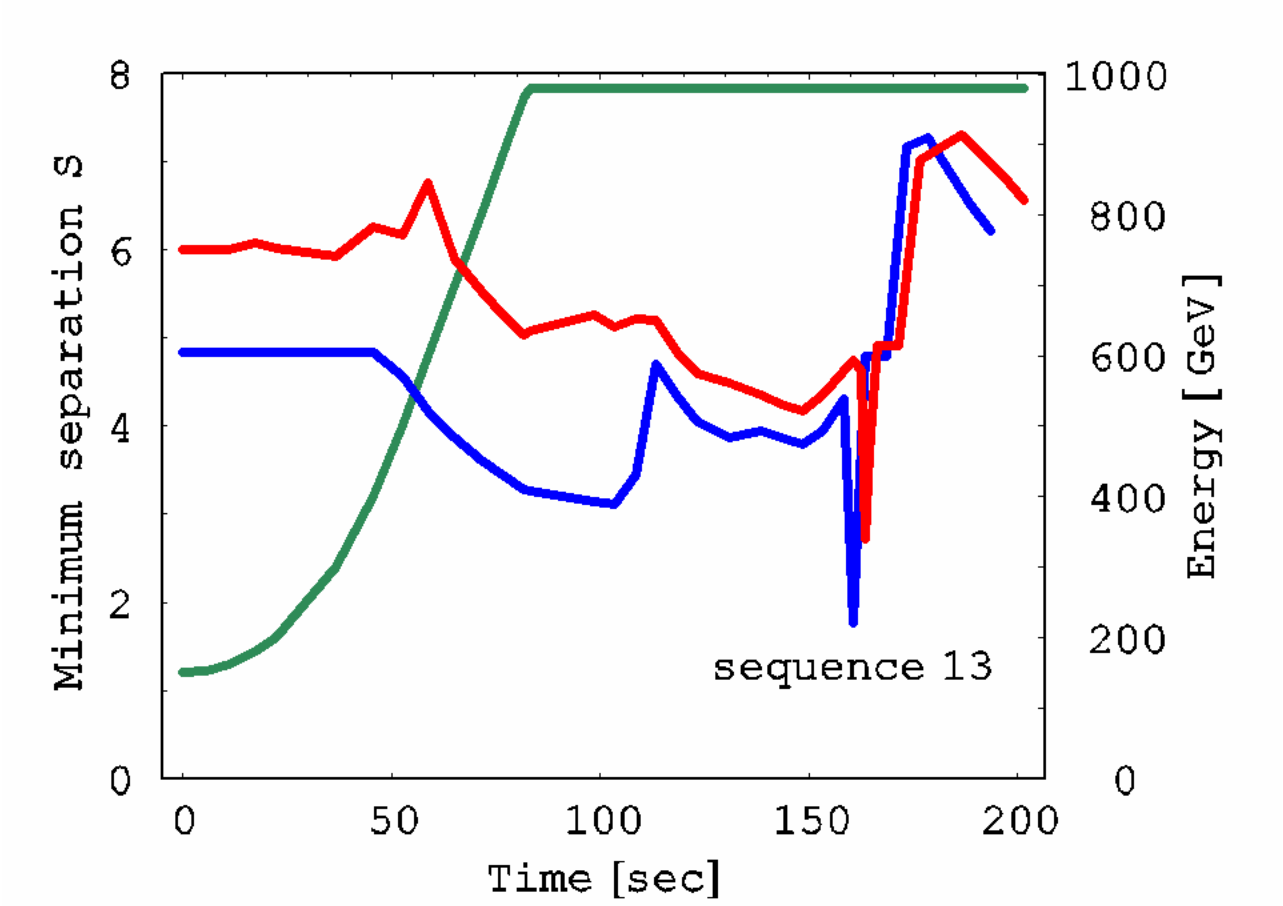

FIG. 7. Minimum radial separation, Eq. (2), on ramp and during the low-beta squeeze. The green line represents the beam energy on the ramp *E(t)*. The blue and red lines represent *S(t)* for the helix configurations used circa January 2002 and August 2004, respectively.

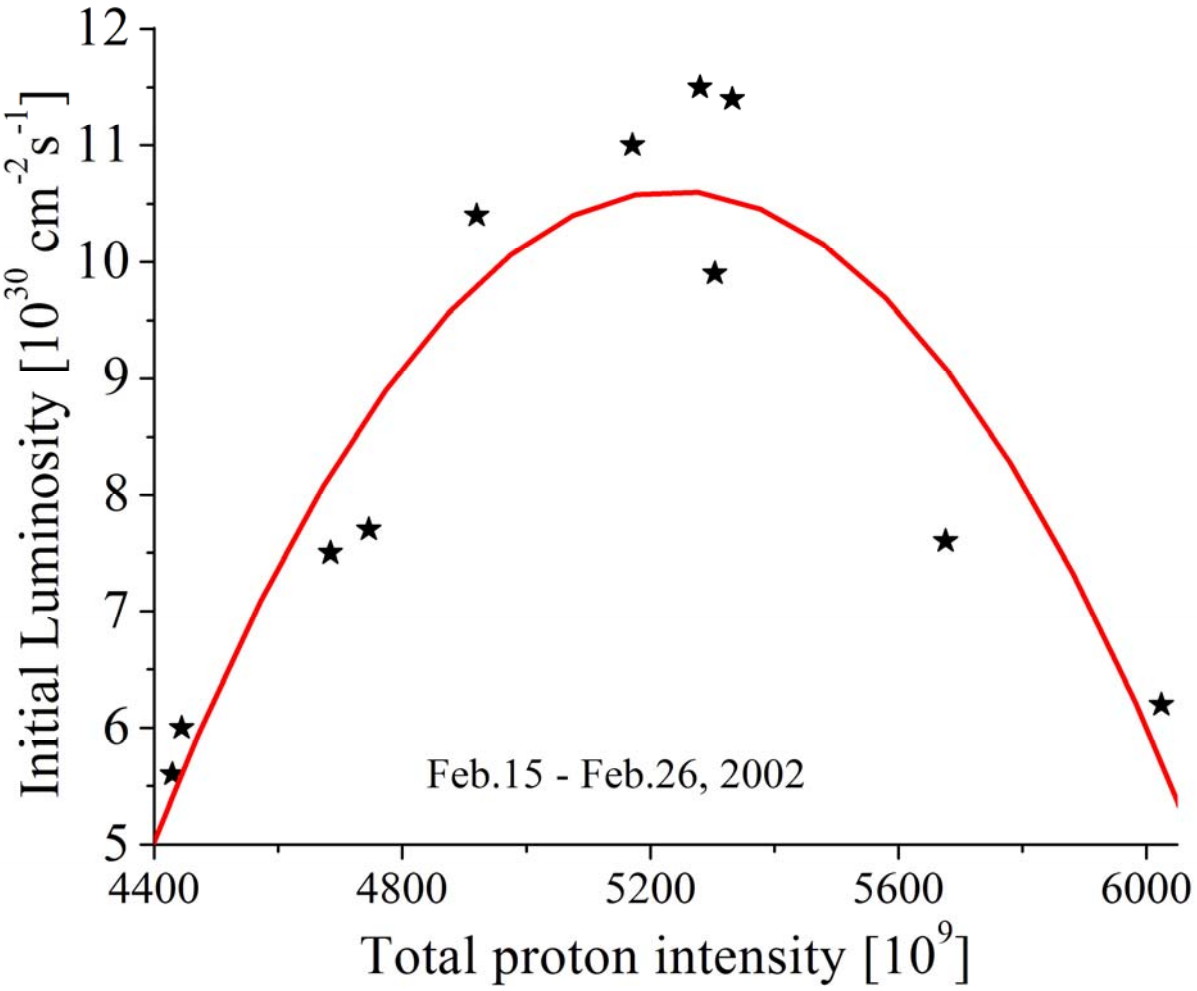

FIG. 8. Average initial luminosity in stores #990-1023 (February 2002) vs total proton intensity. The luminosity reduction for higher proton intensities was caused by larger antiproton losses at sequence 13 of the low-beta squeeze.

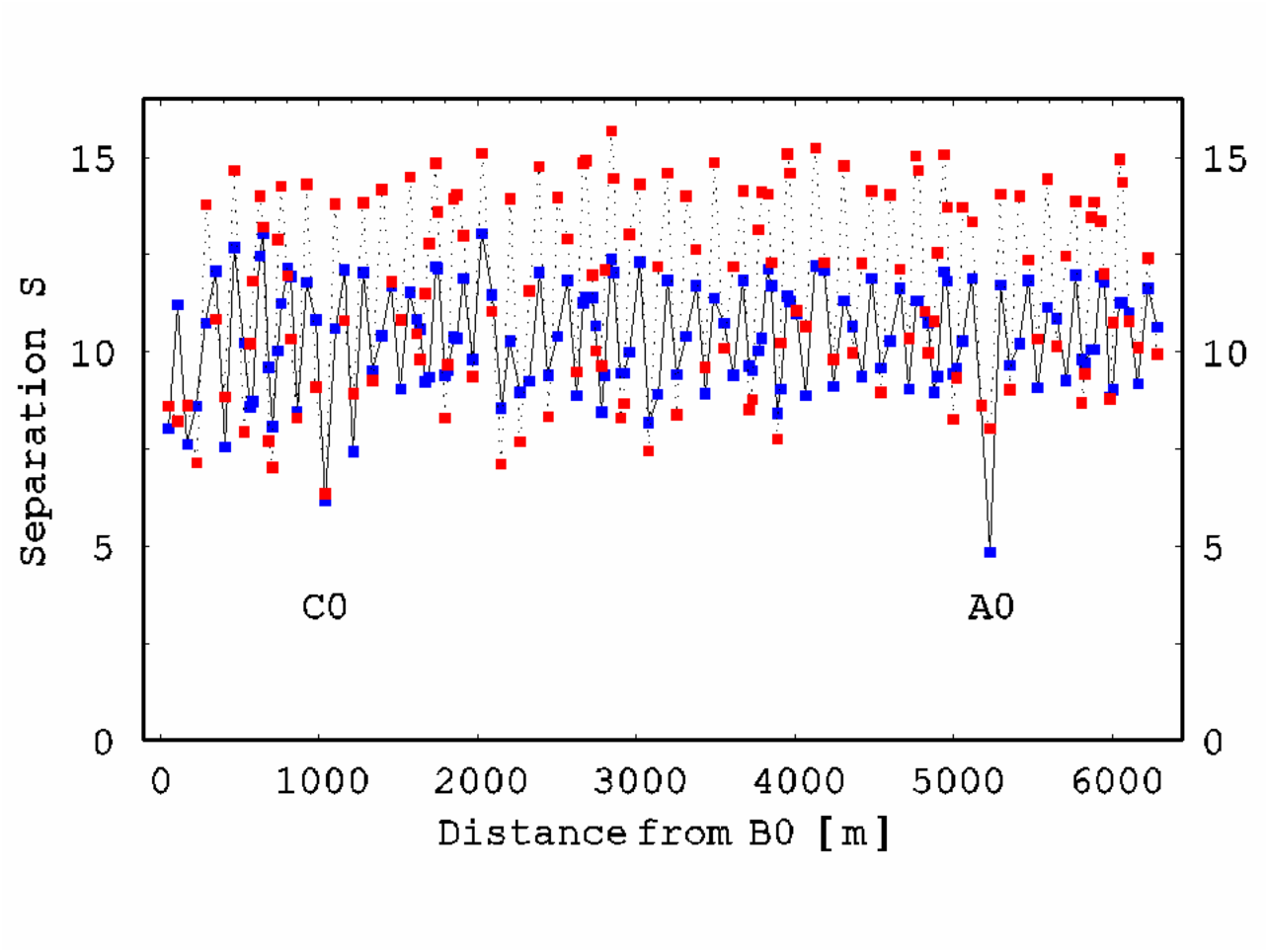

FIG. 9. Radial beam-beam separation S at all possible parasitic interaction points around the Tevatron ring at 150 GeV before (January 2002, blue points) and after the helix modification (May 2002, red points). The longitudinal coordinate z starts at the B0 location.

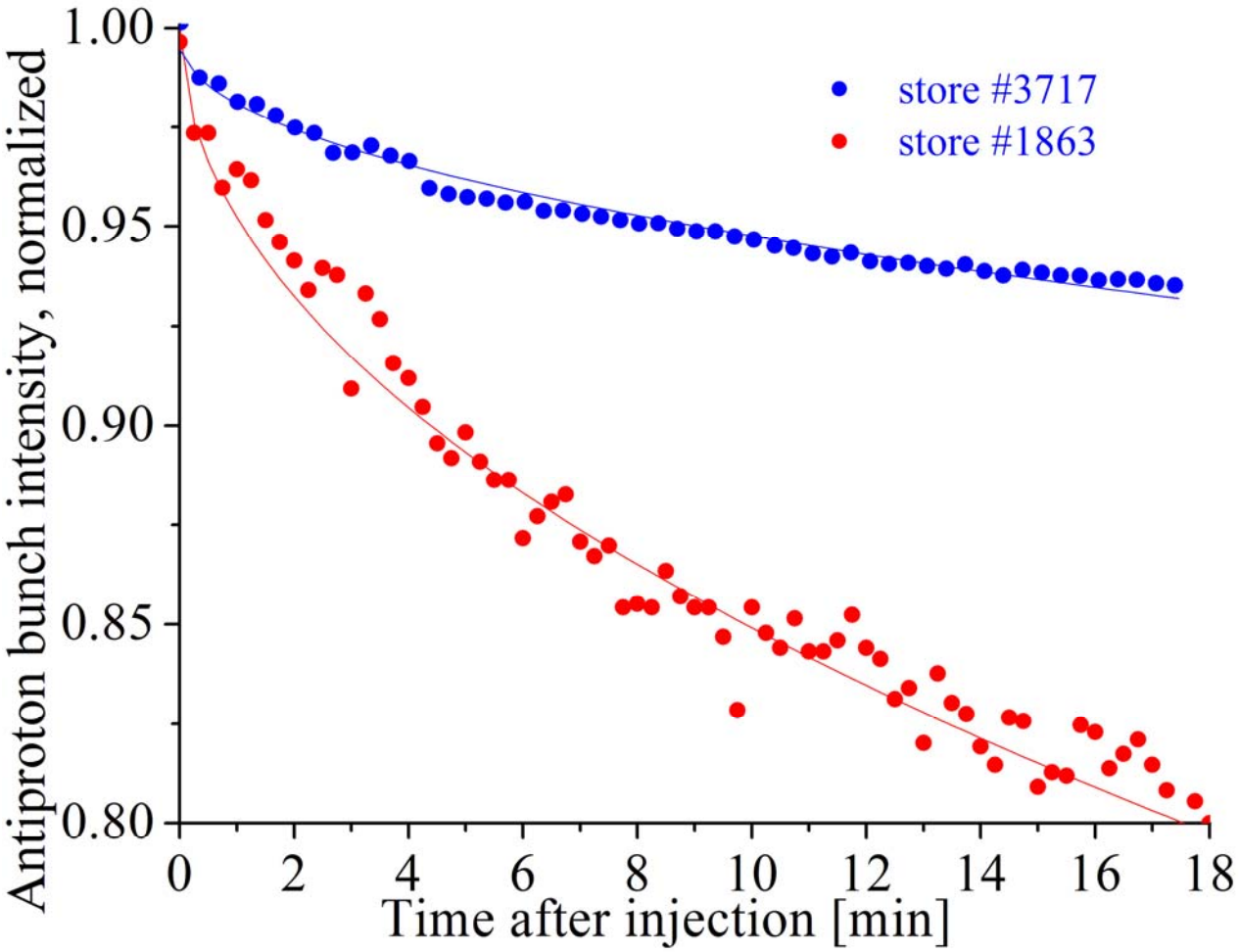

FIG. 10. Decay of (normalized) intensity for antiproton bunch #1at injection. The red dots are for store #1863 (October 16, 2002) and the blue dots are store #3717 (August 8, 2004). The blue and red lines represent fits according to Eq. (6) with parameters N_0=32.5 10^9, τ=7.4 hr and N_0=55.7 10^9, τ=69.8 hr, respectively.

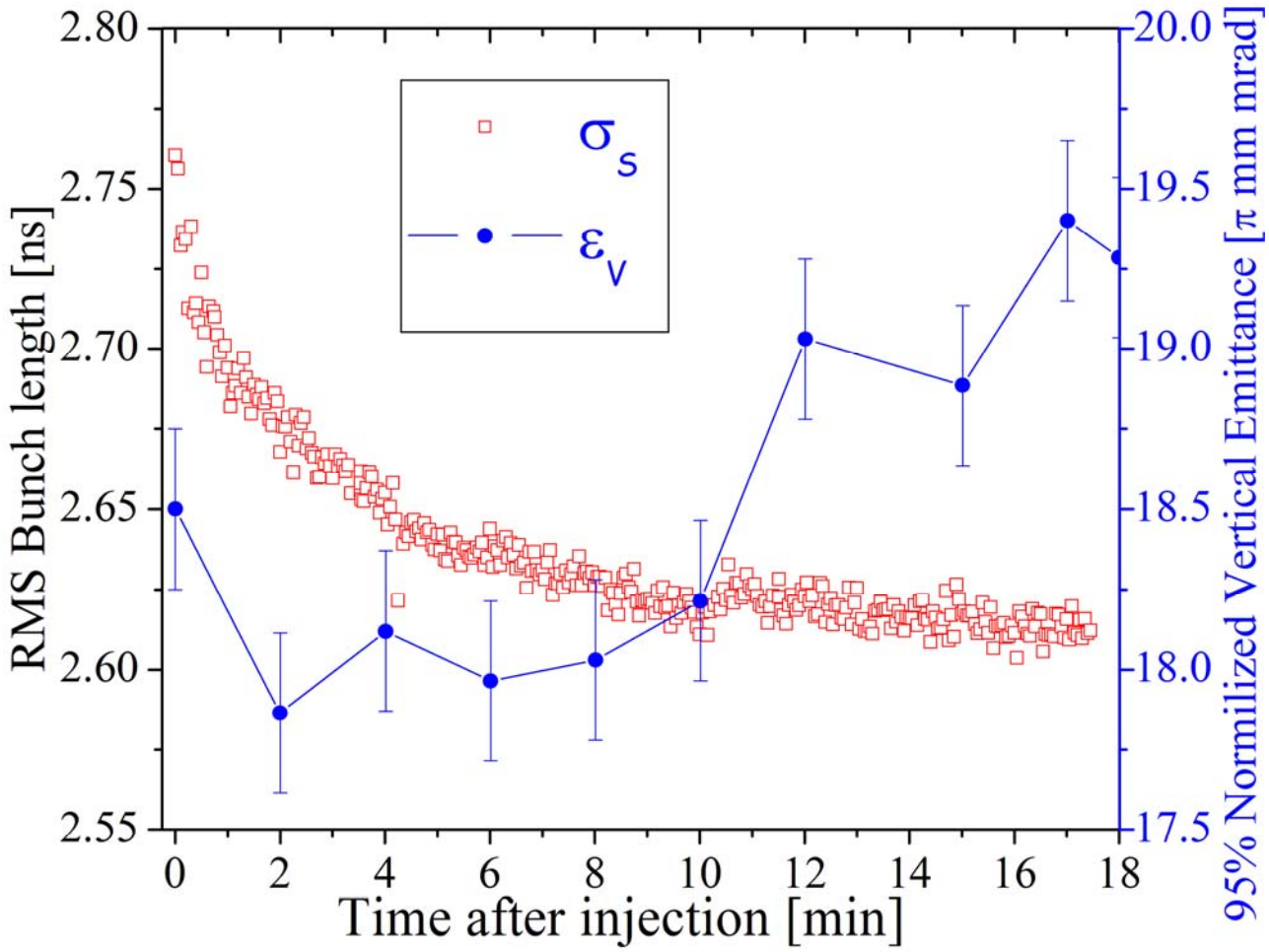

FIG. 11. Time evolution of RMS bunch length (red squares) and 95% normalized vertical emittance of antiproton bunch 1 (blue dots) after injection in store #3717 (August 8, 2004). The error bars represent an RMS systematic error in the flying wire emittance measurements.

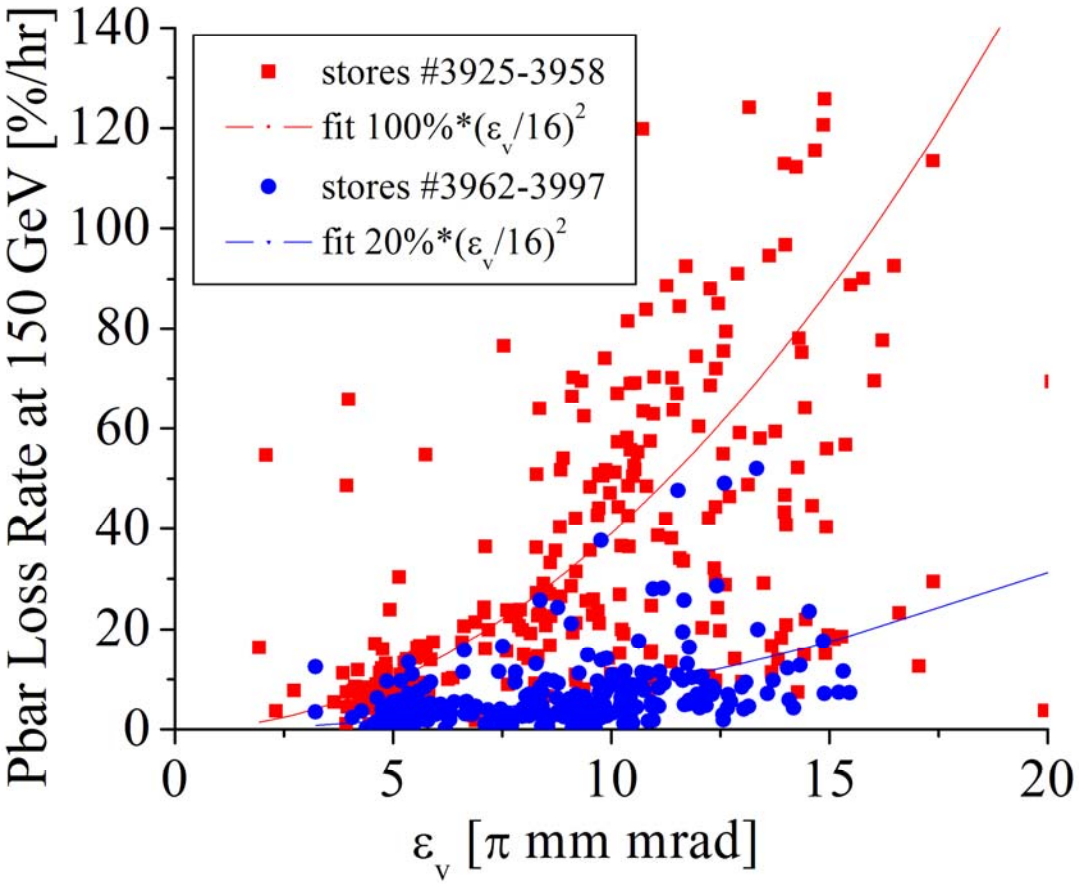

FIG. 12. Antiproton bunch intensity loss rates at injection in units of %/hr vs vertical emittance ε_V. Each data point is the loss rate calculated from an exponential decay fit over the first 2 minutes after bunch injection. The red squares represent all bunches in stores #3925-3958 (January 2005) when vertical and horizontal chromaticities on the antiproton helix were set at approximately Q_x'= 8.0 and Q_y'= 3.5 units. The blue circles show data for all bunches in stores #3962-3997 (February 2005) when the chromaticities were reduced to about 3 units in each plane. The red and blue solid lines are the fits $100[\%/hr]/(\varepsilon_V/16)^2$ and $20[\%/hr]/(\varepsilon_V/16)^2$, respectively.

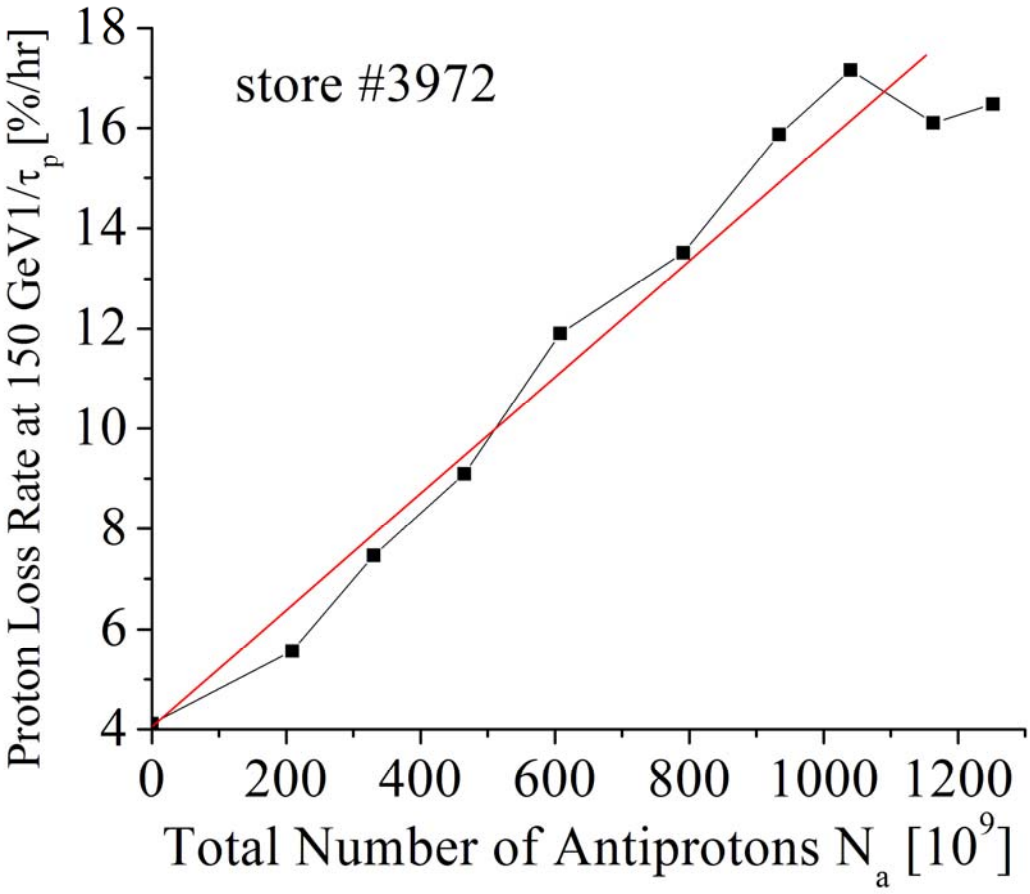

FIG. 13. Proton intensity loss rate at 150 GeV helix in units of %/hr vs total number of antiprotons injected into the Tevatron N_a during shot setup #3972 (February 8, 2005). The points are the results of ordinary exponential decay fits over 2 minutes after each antiproton injection. The solid red line is the linear fit $1/\tau_p[\%/hr]=4+11.6(\ N_a/1000)$.

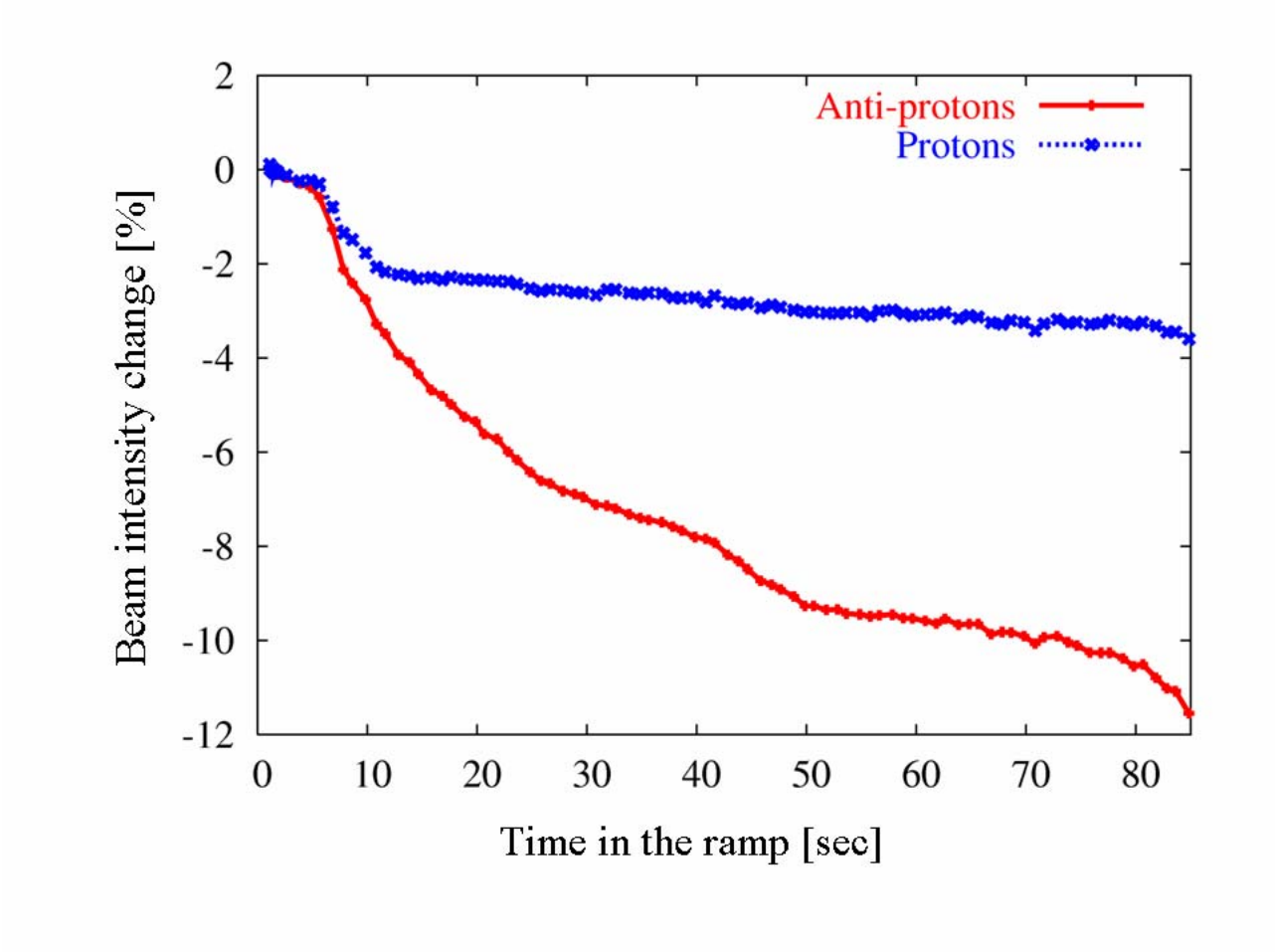

FIG. 14. Normalized proton (blue line) and antiproton (red line) intensity losses on the energy ramp for store #3717 (August 8, 2004). The total bunched beam intensities before the ramp were 10.04 10^{12} and 1.22 10^{12} particles, respectively.

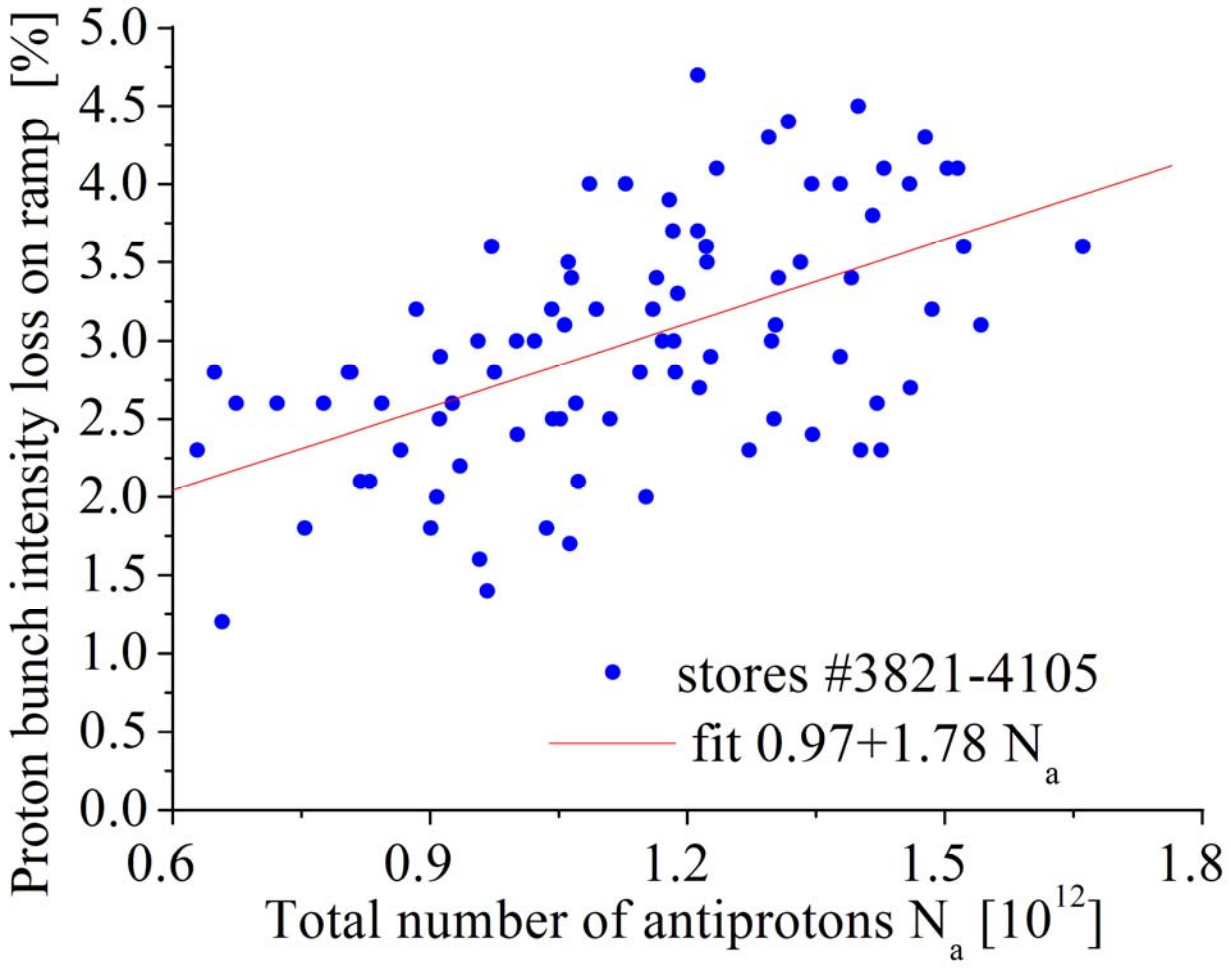

FIG. 15. Relative proton intensity loss on ramp dN_p vs total number of antiprotons N_a in stores #3821-4105 (December 2004 – April 2005). The solid red line is the linear fit $dN_p[\%]=0.97+1.78\ N_a$.

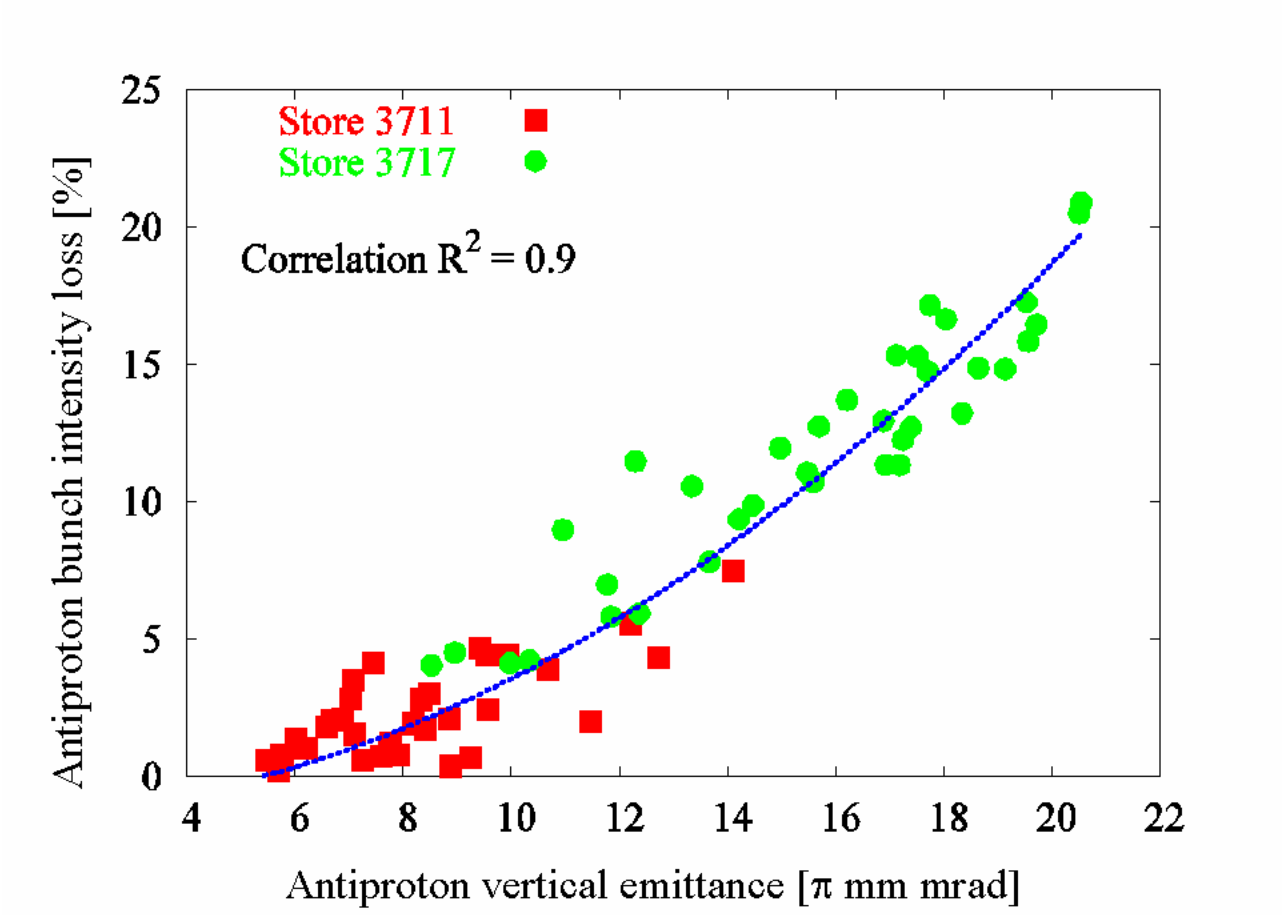

FIG. 16. Antiproton bunch intensity loss on the ramp vs antiproton vertical emittance for all bunches in stores #3711 (August 5, 2004) (red squares) and #3717 (August 8, 2004) (green circles). The dotted line represents the fit $dN_a[\%] \approx 20(\varepsilon_a/20)^2$.

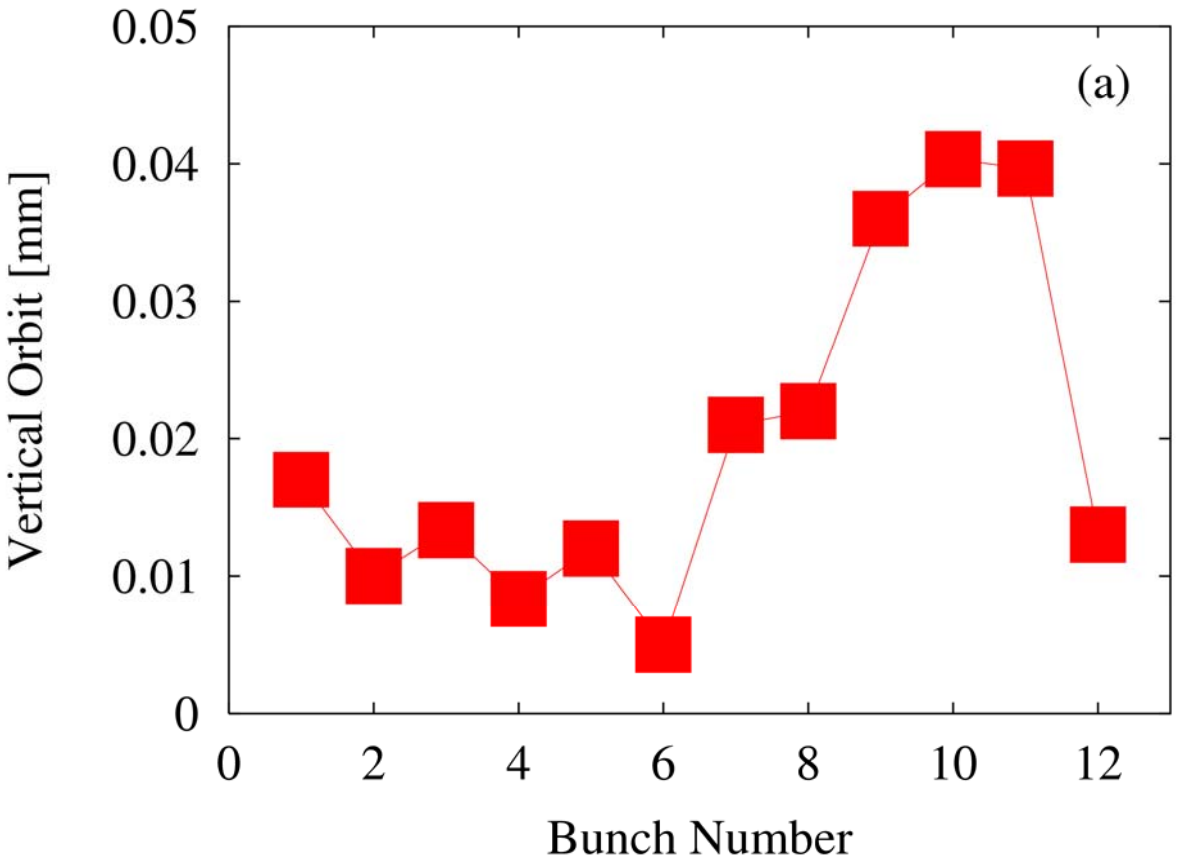
(a)
Vertical Orbit [mm]
0.05
0.04
0.03
0.02
0.01
0
0
2
4
6
8
10
12
Bunch Number

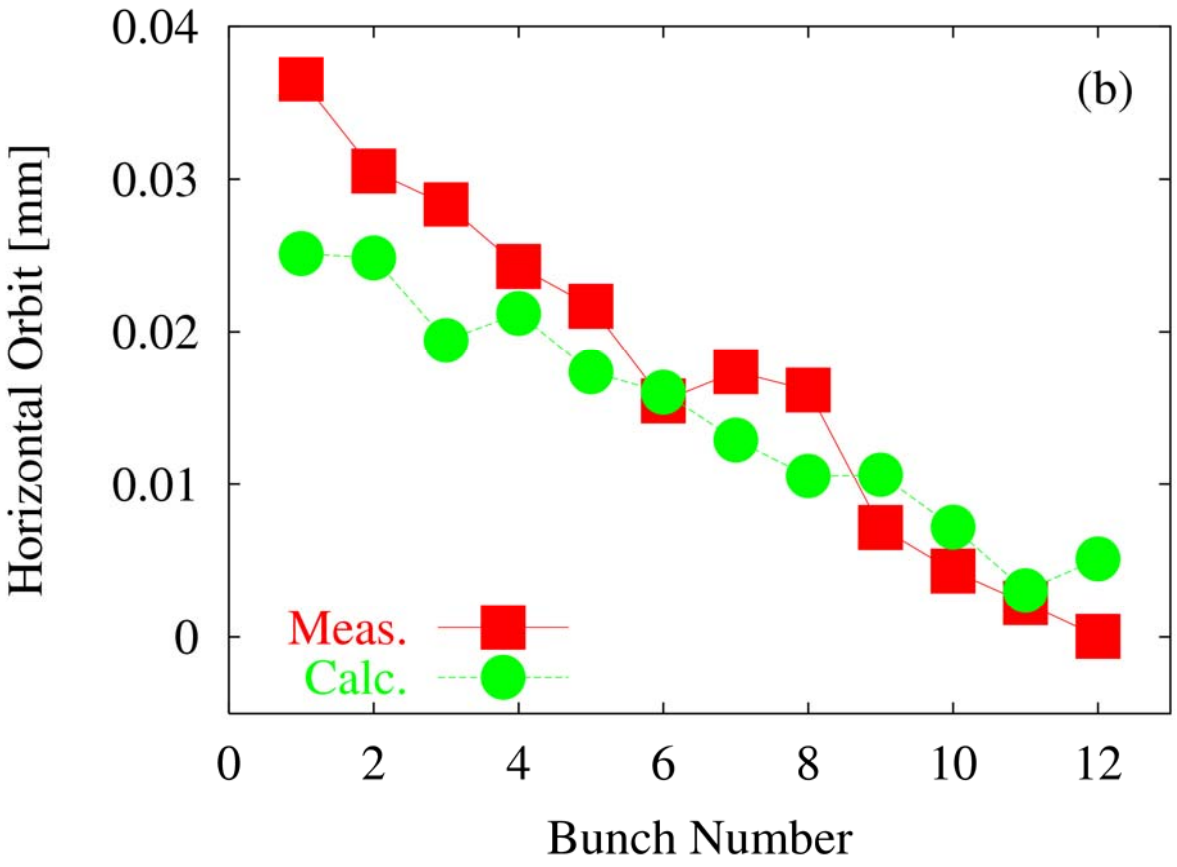
0.04
0.03
0.02
0.01
0
Horizontal Orbit [mm]
(b)
Meas.
Calc.
0
2
4
6
8
10
12
Bunch Number

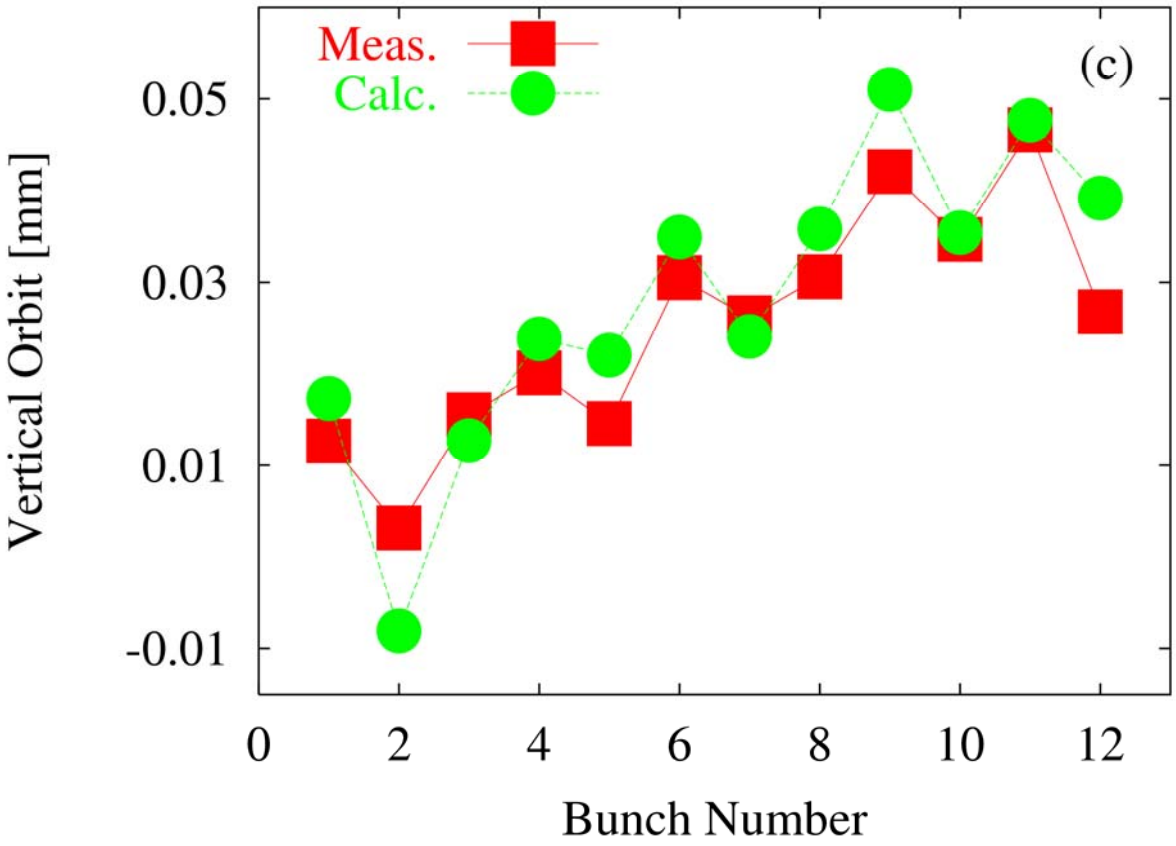

FIG. 17. Antiproton orbit variations along the bunch train: (a) vertical positions measured by flying wires at 150 GeV in store #3678 (July 27, 2004); for comparison, the RMS vertical betatron size of 15 π mm mrad beam at the location of the flying wire is about 1.1 mm; (b) horizontal positions measured by synchrotron radiation monitor in collisions in store #3530 (May 23, 2004) (red squares) and calculated (green circles); for comparison, RMS horizontal betatron size of 15 π mm mrad beam at the location of the monitor is equal to 0.3 mm; (c) vertical positions measured by synchrotron radiation monitor in collisions in store #3530 (May 23, 2004) (red squares) and calculated (green circles); for comparison, RMS vertical betatron size of 15 π mm mrad beam at the location of the monitor is equal to 0.5 mm.

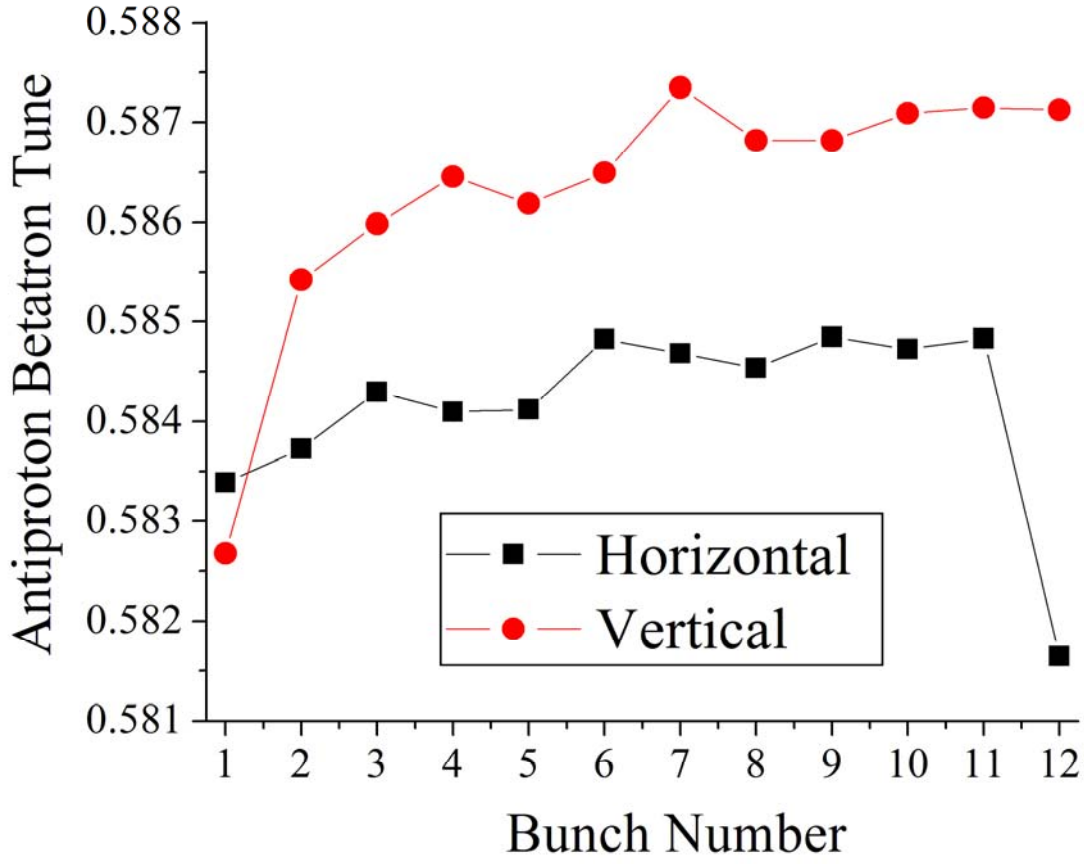

FIG. 18. Horizontal and vertical antiproton tunes versus bunch number within a 12 bunch train measured by 1.7 GHz Schottky monitor at T=3 hours into the store #3678 (July 27, 2004). The data were taken over a period of three hours, starting three hours after the beginning of the store and extrapolated linearly to the time T=3 hours into the store.

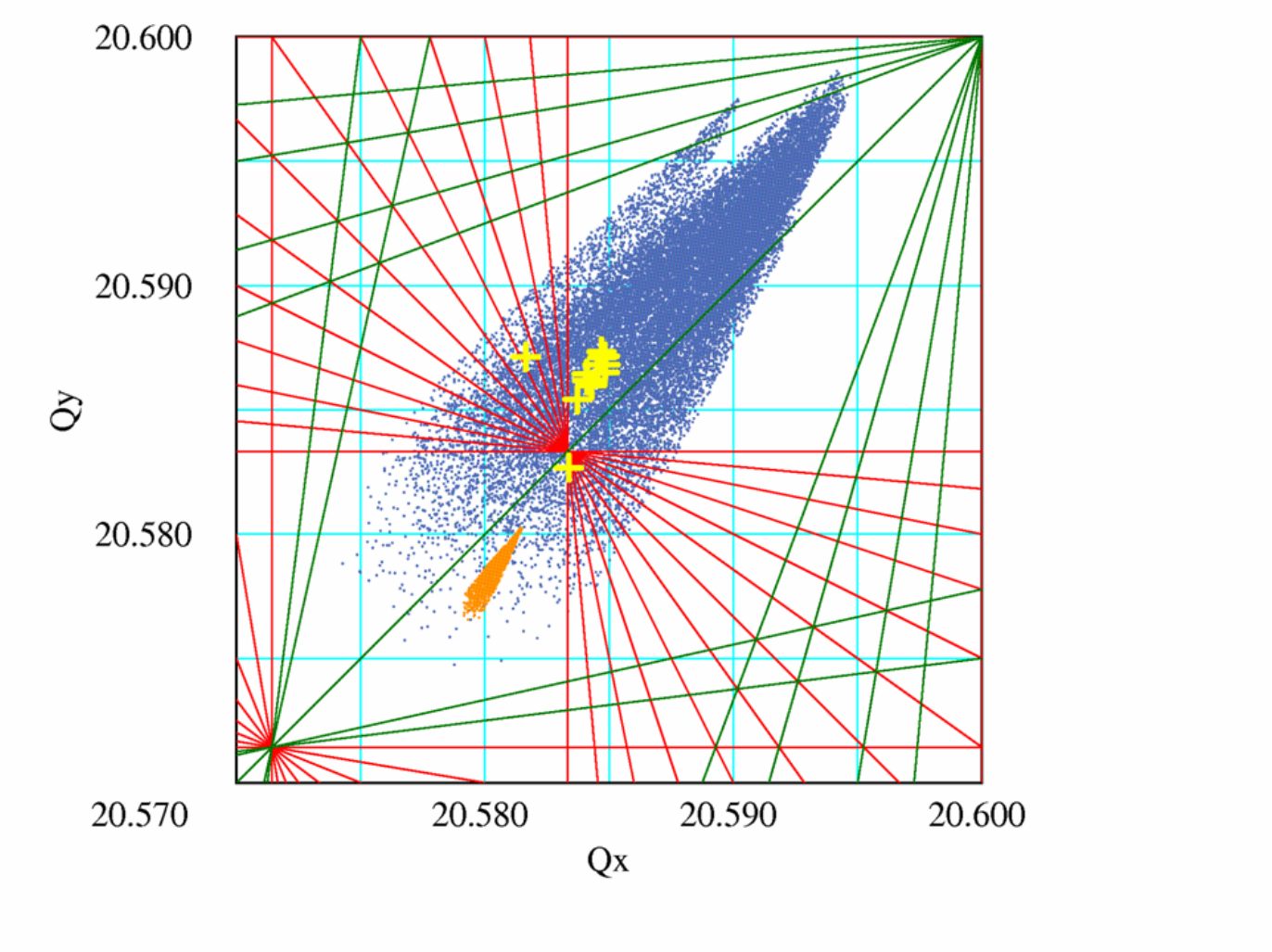

FIG. 19. Tevatron proton and antiproton tune distributions superimposed onto a resonance line plot. The red and green lines are various sum and difference tune resonances. The yellow crosses are the weighted average tunes for each antiproton bunch as measured by the 1.7 GHz Schottky monitor in store #3678 (July 27, 2004). The blue (pink) dots are the calculated tune distributions for all 36 antiproton (proton) bunches. The tune spread for each bunch is calculated for particles up to 6σ amplitude taking into account the measured intensity and emittance parameters.

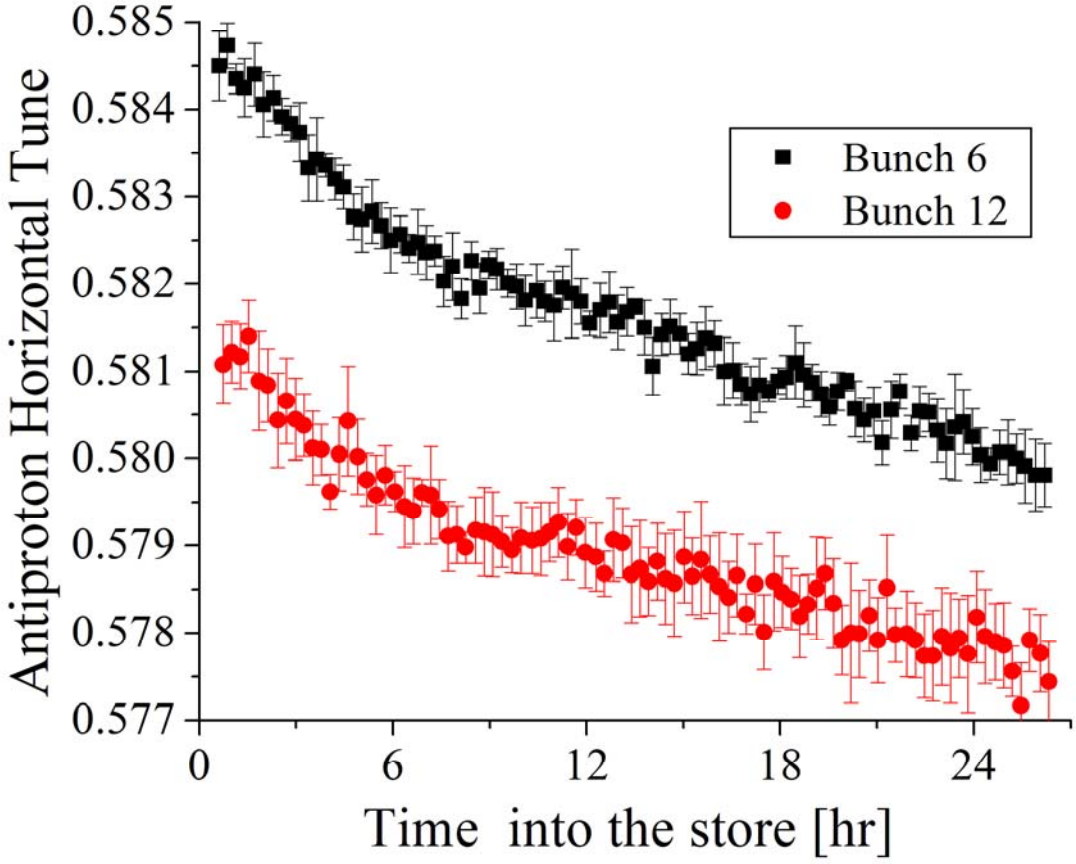

FIG. 20. Time evolution of the horizontal tune for antiproton bunches #6 and #12 during store #3678 (July 27-28, 2004).

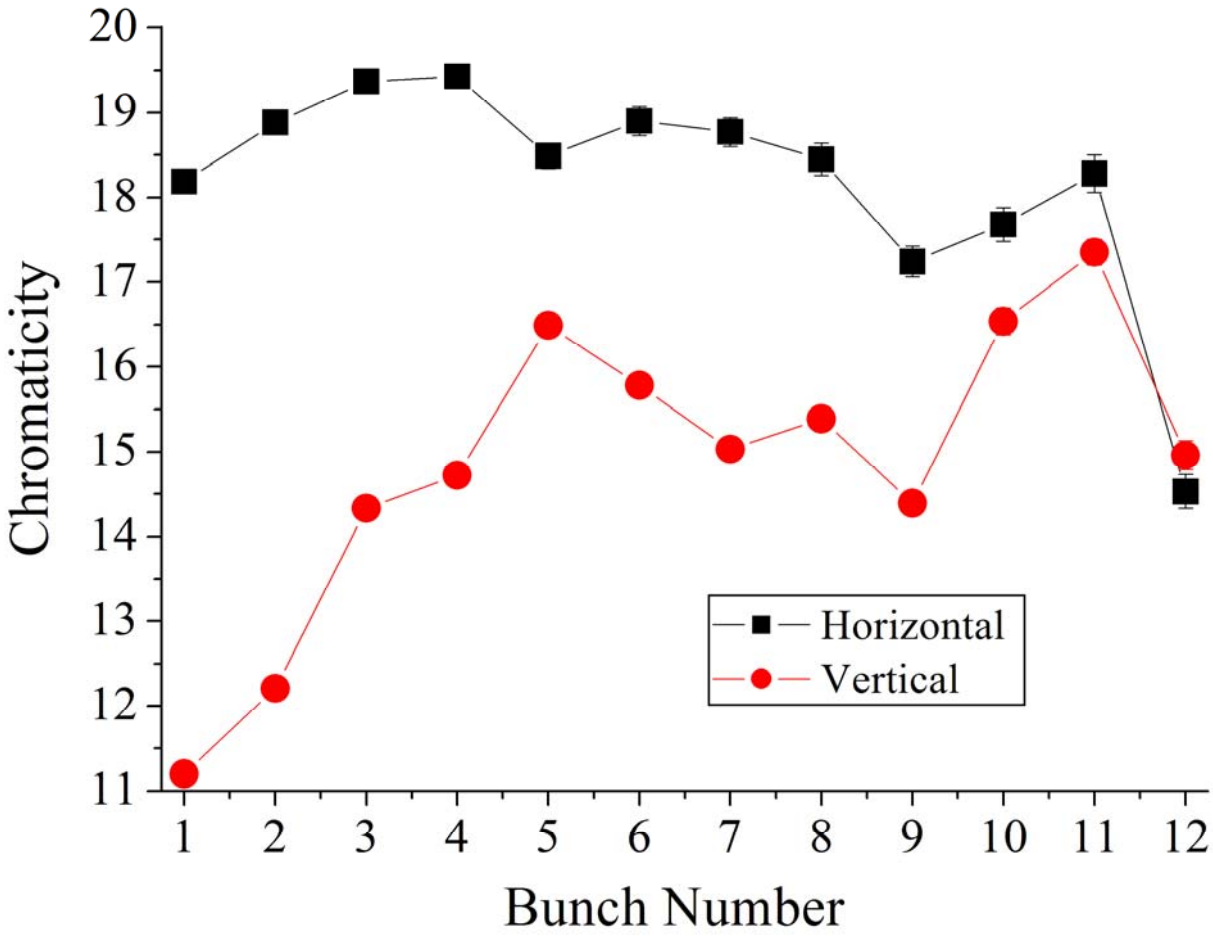

FIG. 21. Antiproton chromaticities measured by the 1.7 GHz Schottky monitor versus bunch number for store #3678 (July 27-28, 2004). The chromaticities were assumed to be constant, and so the measurements were averaged over the entire store. The symbol size reflects the size of the statistical error bars.

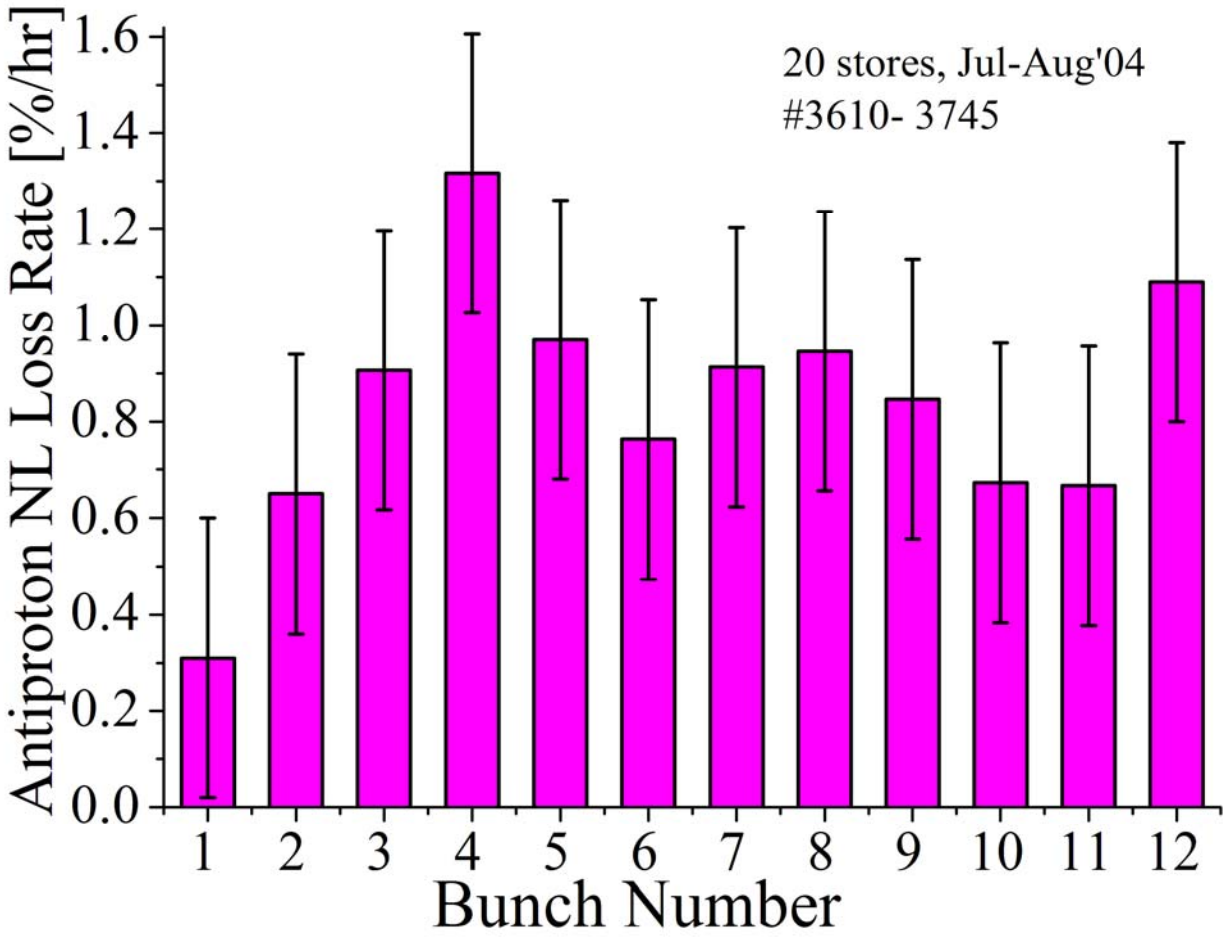

FIG. 22. Variation of antiproton bunch intensity loss rates during the first 2 hours of HEP stores #3610-3745 (July –August 2004) along bunch train. Only one bunch train is presented due to the three-fold symmetry of the trains. The error bars reflect the RMS differences from store-to-store.

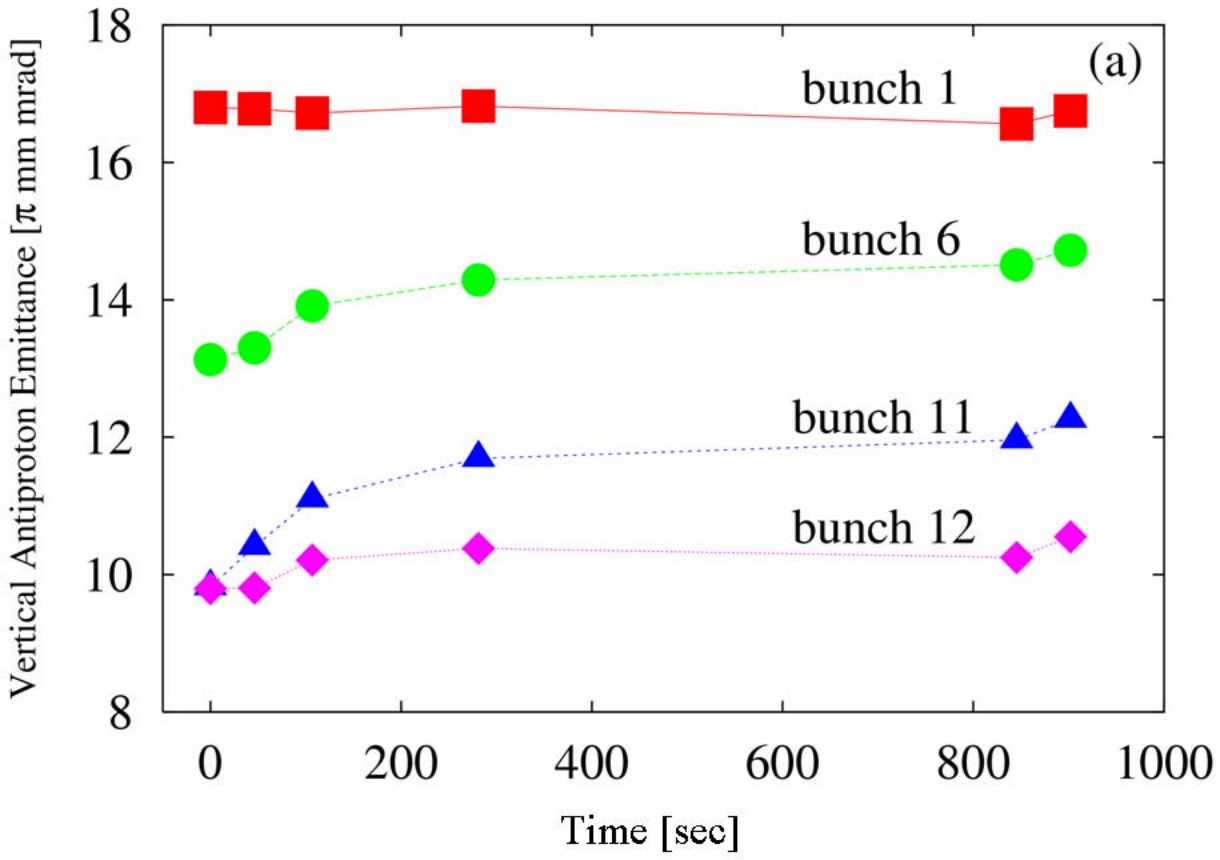
18
16
14
12
10
8
0
200
400
600
800
1000
Vertical Antiproton Emittance [π mm mrad]
Time [sec]
(a)
bunch 1
bunch 6
bunch 11
bunch 12

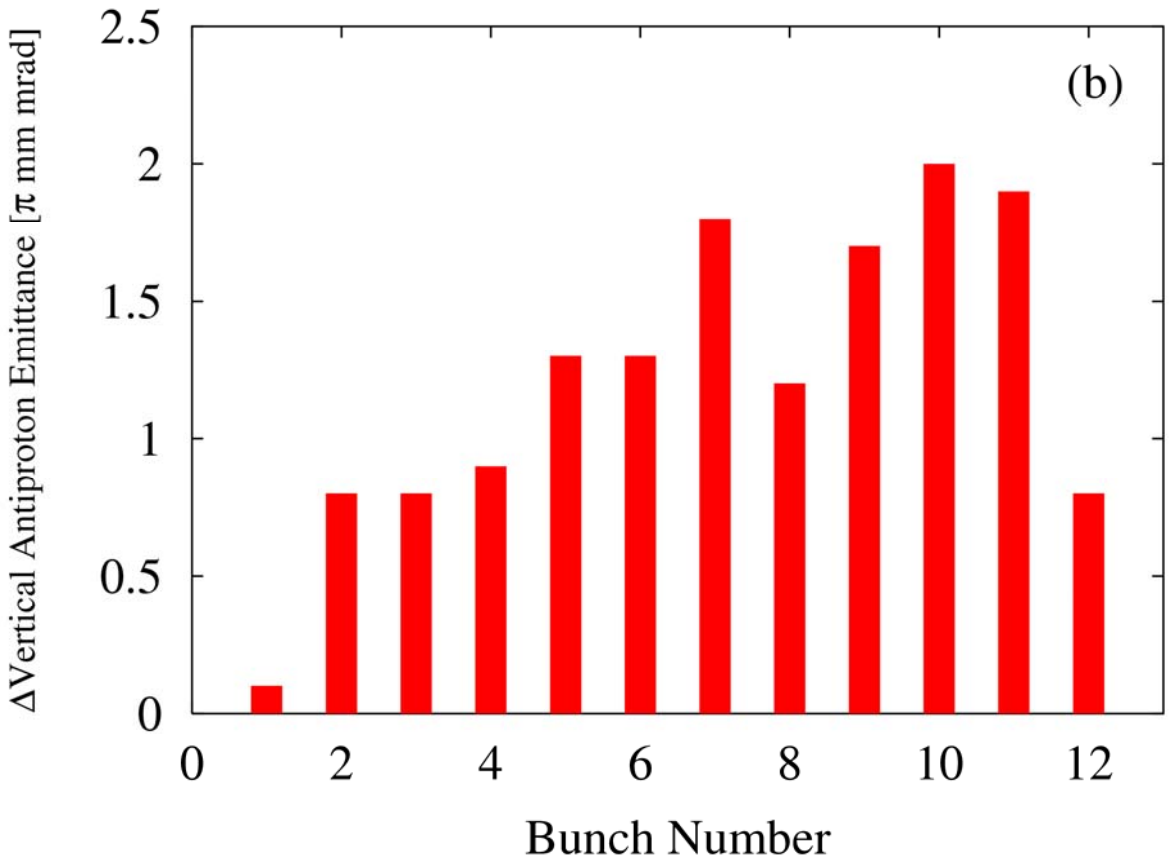

FIG. 23. Antiproton vertical emittance growth after collisions were initiated in store #3554 (June 2, 2004): (a) time evolution for bunches 1, 6, 11 and 12, (b) vertical emittance growth after the first 15 minutes of collisions. (b) also illustrates the "scallop" - the two bunches at the ends of the train show smaller emittance growth than bunches in the middle of train. Due to the three-fold symmetry, only the one train of bunches presented.

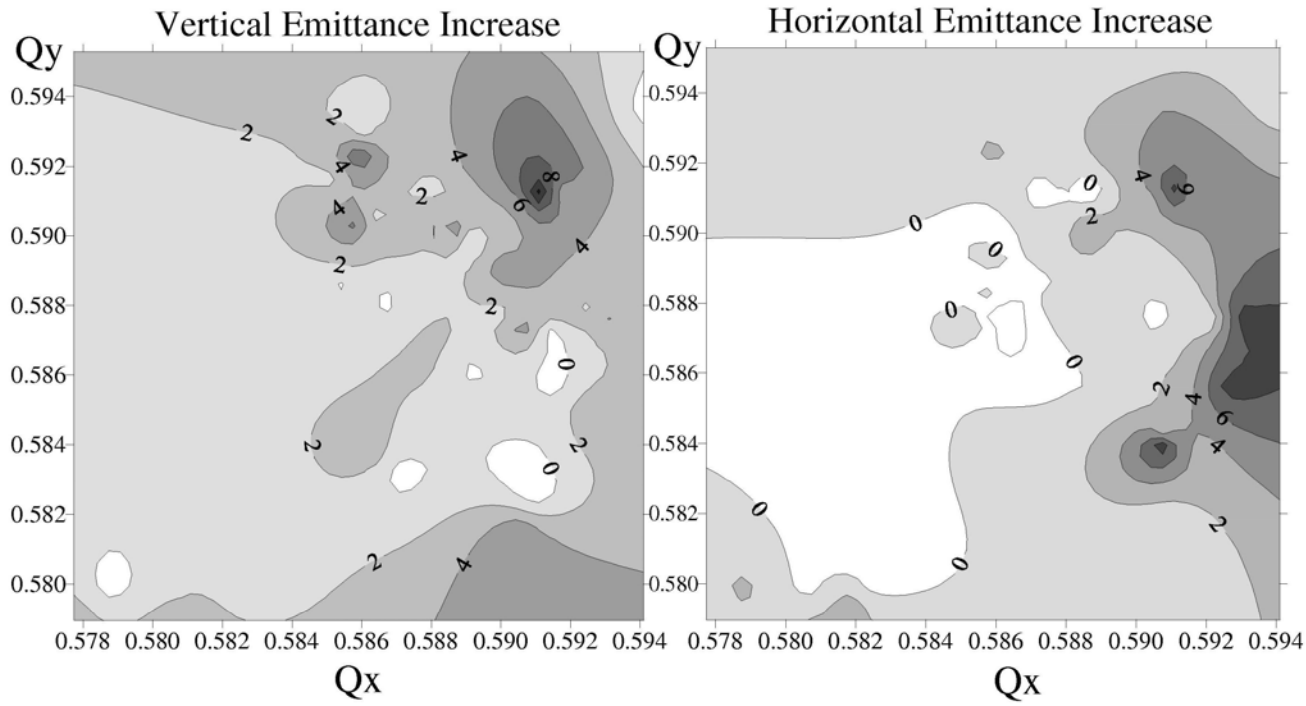

FIG. 24. Dependence of the antiproton emittance blowup early in HEP stores on the antiproton tunes for HEP stores #3130-3929 (128 stores, January 2004 to January 2005). The contour lines represent the maximum (among all bunches) emittance increase during the first 15 minutes of collisions in units of π mm mrad. The average betatron tunes $Q_{x,y}$ are measured by the 1.7 GHz Schottky monitors gated on all 36 antiproton bunches simultaneously.

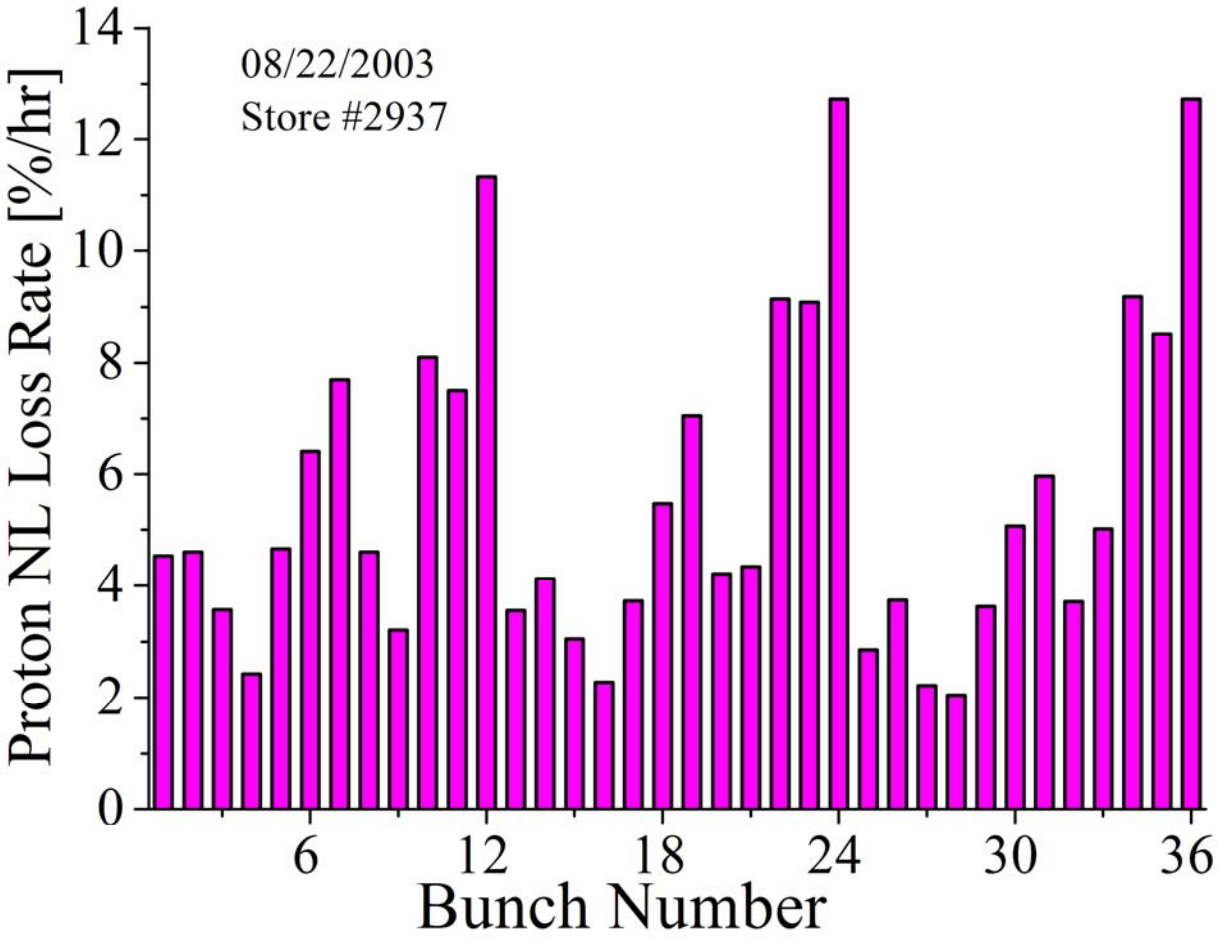

FIG. 25. Non-luminous loss rate of the 36 proton bunches at the beginning of store #2973 (August 22, 2003).

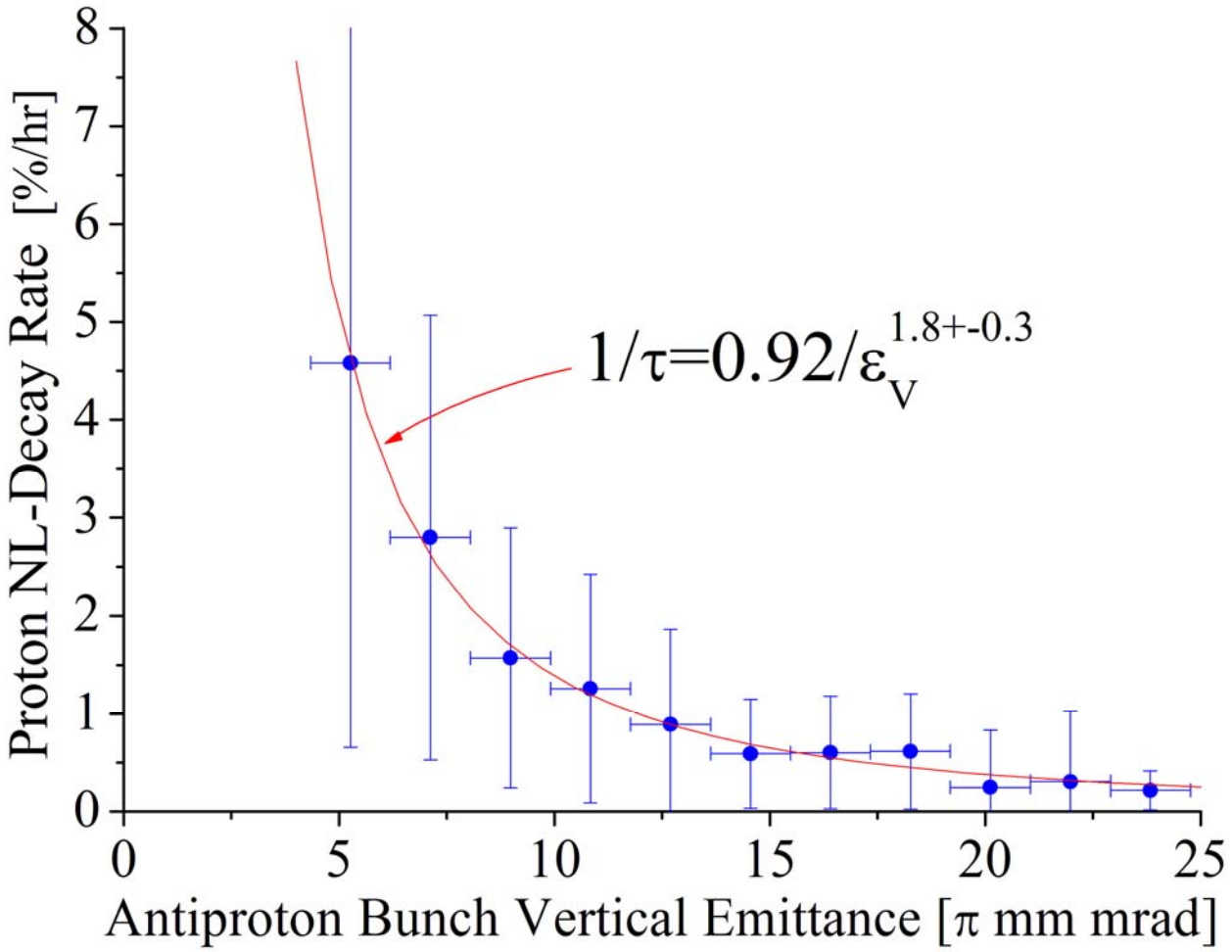

FIG. 26. Non-luminous loss rates of proton bunches at the start of stores vs vertical emittance of the corresponding colliding antiproton bunches. The data was taken for stores #3821-3997 (51 stores, December 2004–February 2005). The horizontal error bars show the emittance bin size for the statistical analysis. The vertical error bars represent the RMS rate variation averaged over all proton bunches within each bin. The red line is the fit $1/\tau_p[1/hr]=0.92/\varepsilon_a^{1.8}$.

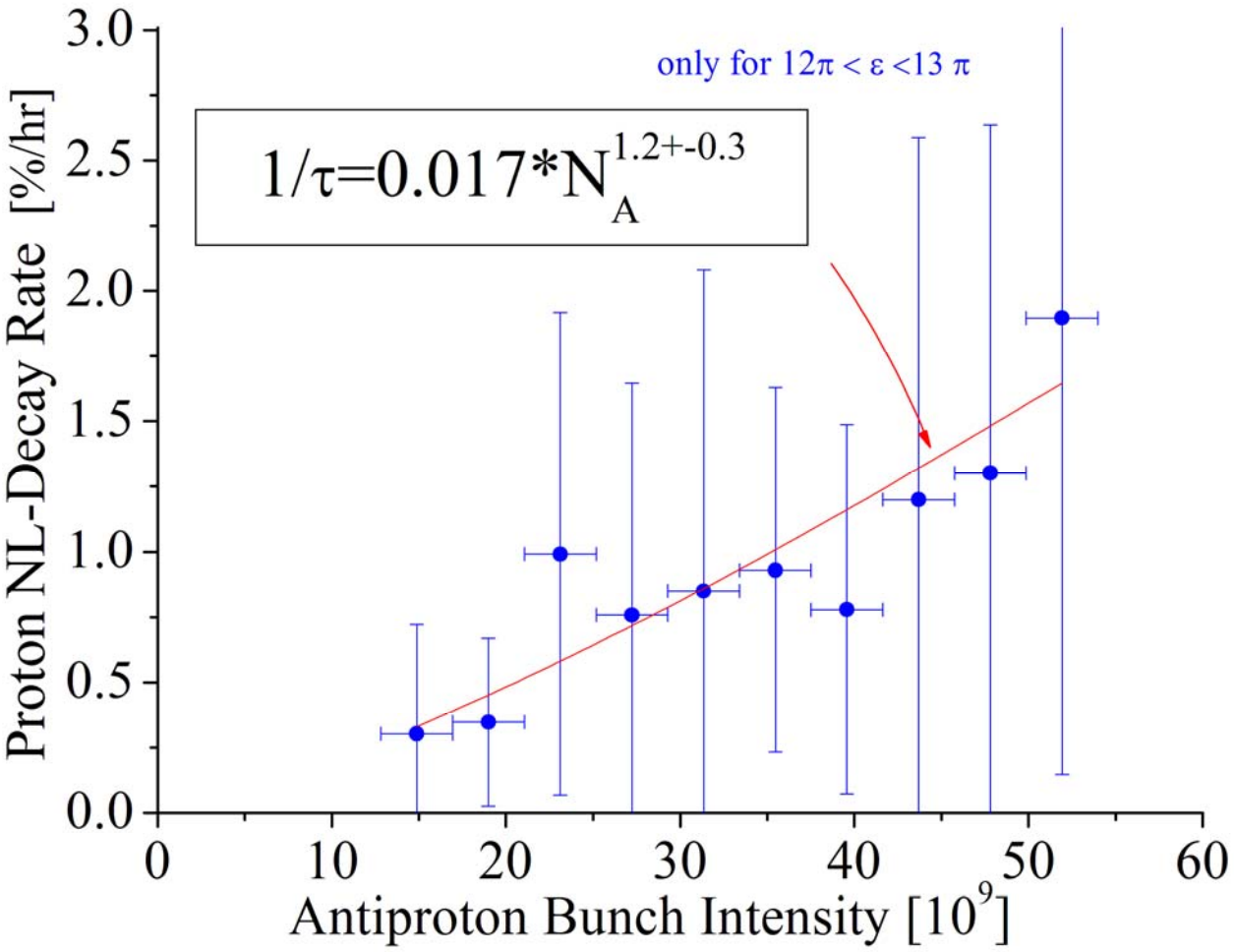

FIG. 27. Non-luminous loss rate of proton bunches vs intensity of the antiproton bunches colliding with them. The data was taken for stores #3821-3997 (51 stores, December 2004–February 2005) The horizontal error bars show the bin size. The vertical error bars represent the RMS rate variations over all proton bunches that collided with antiproton bunches whose emittances were within the range of 12 to 13 π mm mrad . The red line is the fit $1/\tau_p[\%/hr]=0.017\ N_a^{1.2}$.

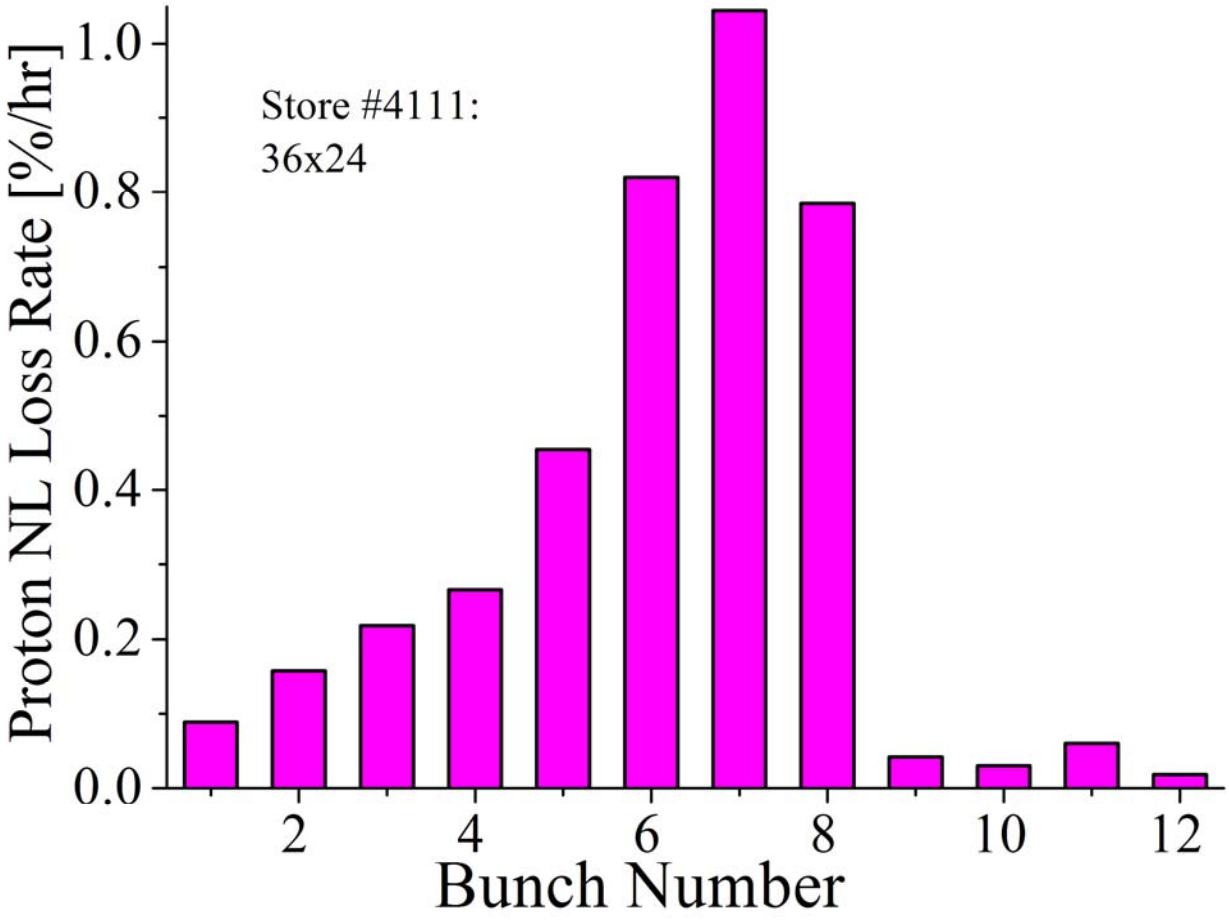

FIG. 28. Non-luminous loss rate of proton bunches #1-12 in the first 3 hours of 36x24 store #4111 (April 25, 2005). Proton bunches #1-4 collided head-on with 27 π mm mrad emittance antiproton bunches at D0 and with 7 π mm mrad bunches at CDF. Proton bunches #5-8 collided head-on with 4 π mm mrad bunches at CDF, but had no collisions at D0. Proton bunches #9-12 had no head-on collisions at either IP. Bunches #10-12 did not experience any encounters with antiprotons at the parasitic crossings nearest to the IPs, while bunches #8-9 had only one nearest parasitic crossing at each IP.

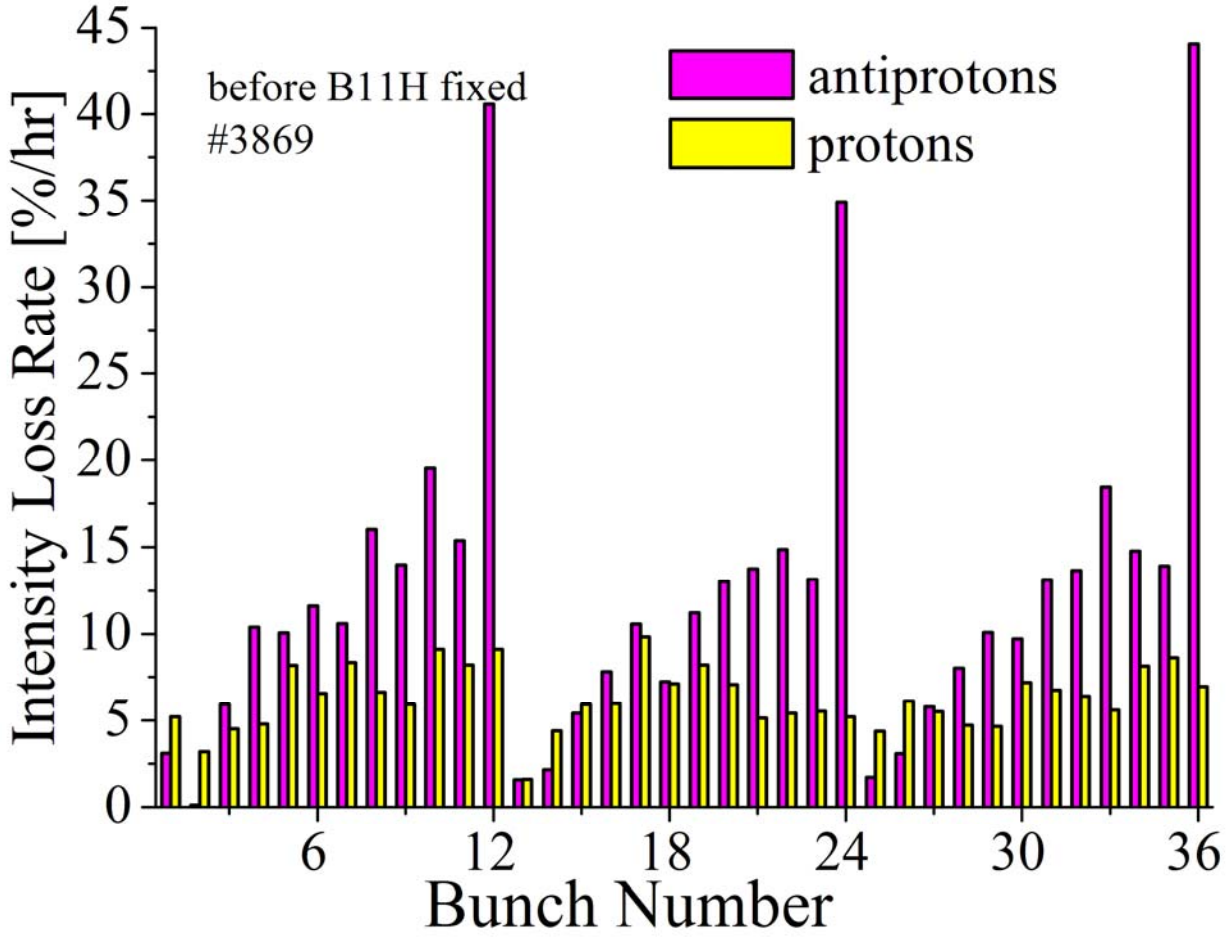

FIG. 29. Intensity loss rates of antiprotons (magenta) and protons (yellow) in the first 20 minutes of store #3869 (December 20, 2004) when a problem with an electrostatic high-voltage separator caused the beams to be separated by 90 μm at the main IPs.

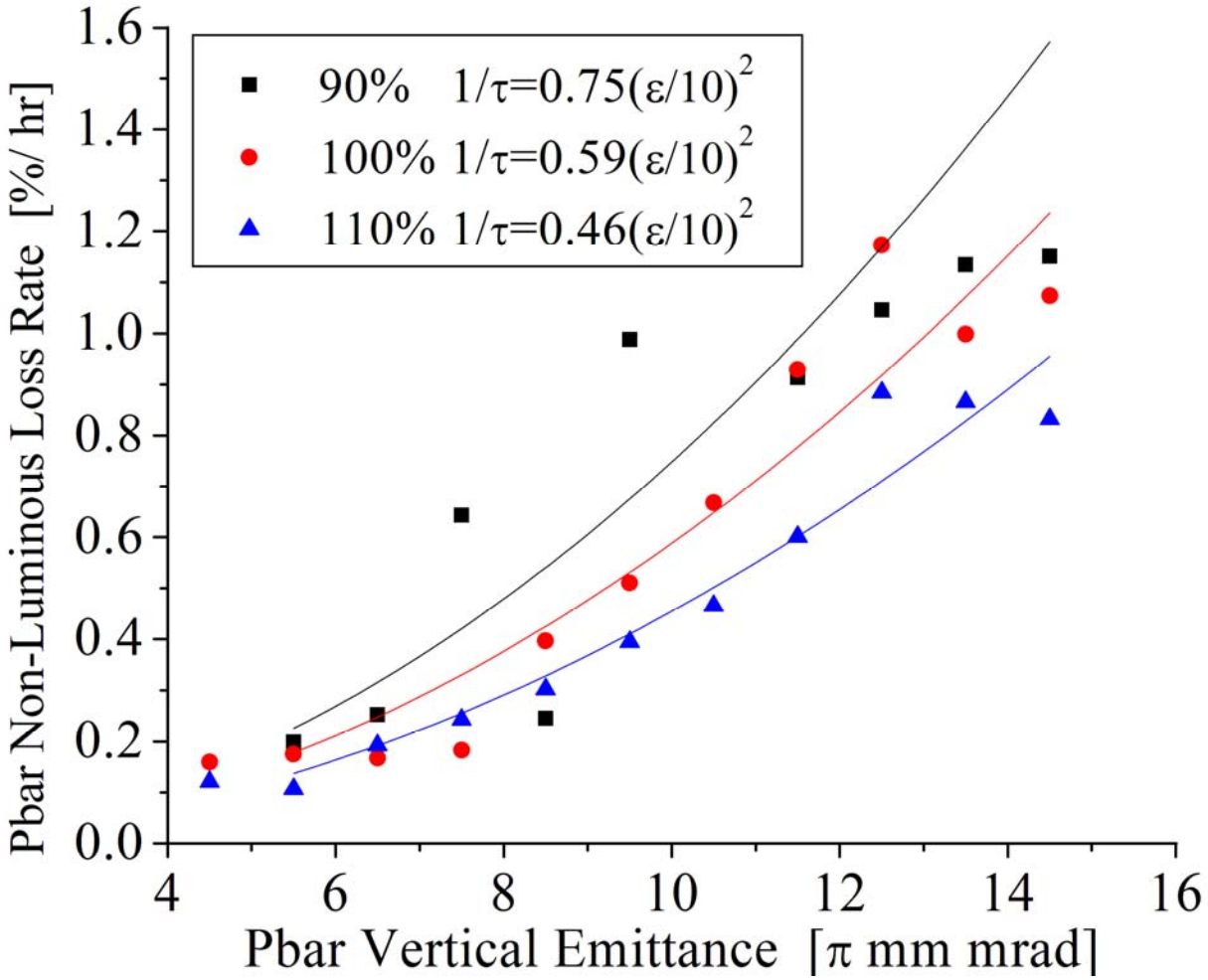

FIG. 30. Dependence of the non-luminous loss rate of antiproton bunch intensity at the start of HEP stores vs their vertical emittances. The data was taken for stores #4021-4109 (35 stores, March-April 2005). Each point is an average loss rate for all bunches having emittances within a 1 π mm mrad bin size. The red circles indicate the 18 stores with nominal (100% helix) separator settings. The black squares show the 6 stores with smaller (90% of nominal) beam separation, while the blue triangles represent the 11 stores with larger (110% of nominal) beam separation. The solid lines represent fits of the form $1/\tau_a \propto \varepsilon_a^2$.

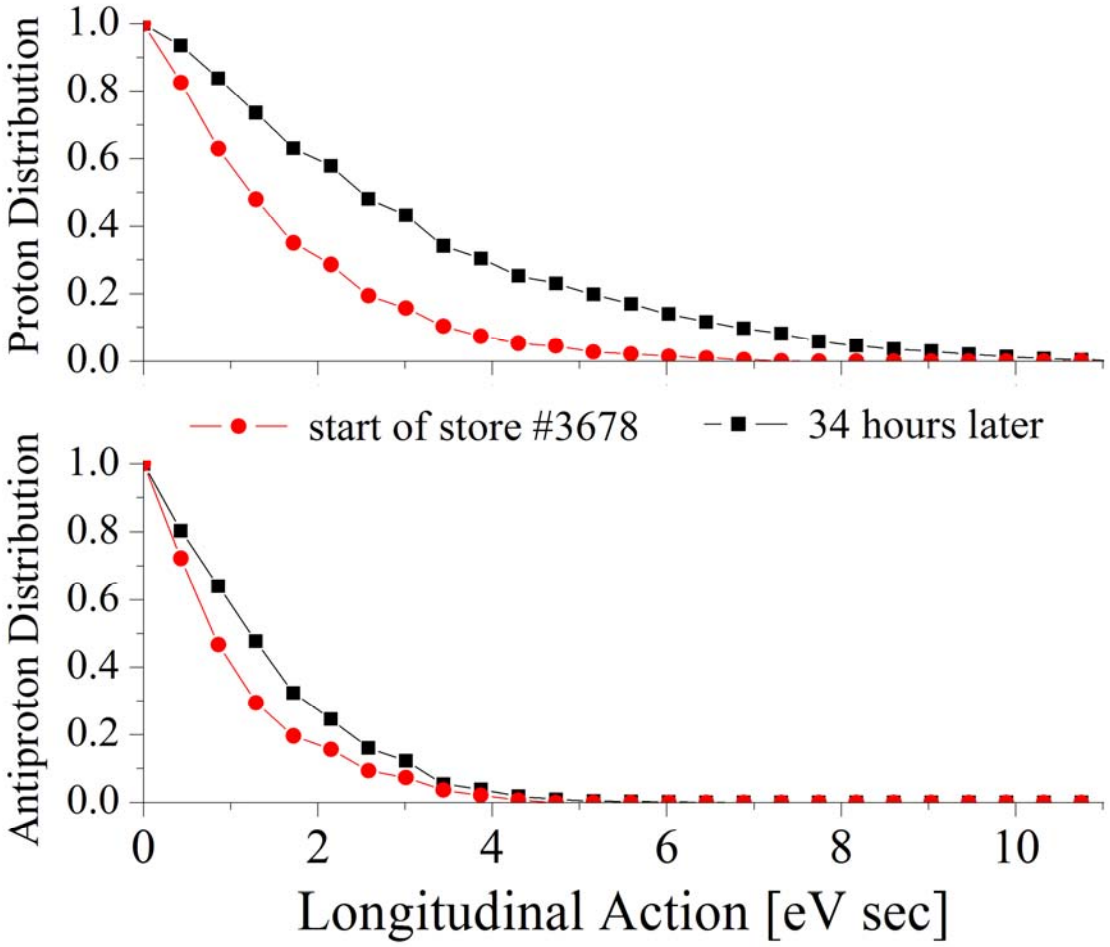

FIG. 31. Normalized proton (a) and antiproton (b) longitudinal distribution functions vs longitudinal action in store #3678 (July 27, 2004). The red circles represent distributions half an hour after the start of the store, while the black squares show them 34 hours later at the very end of the store.

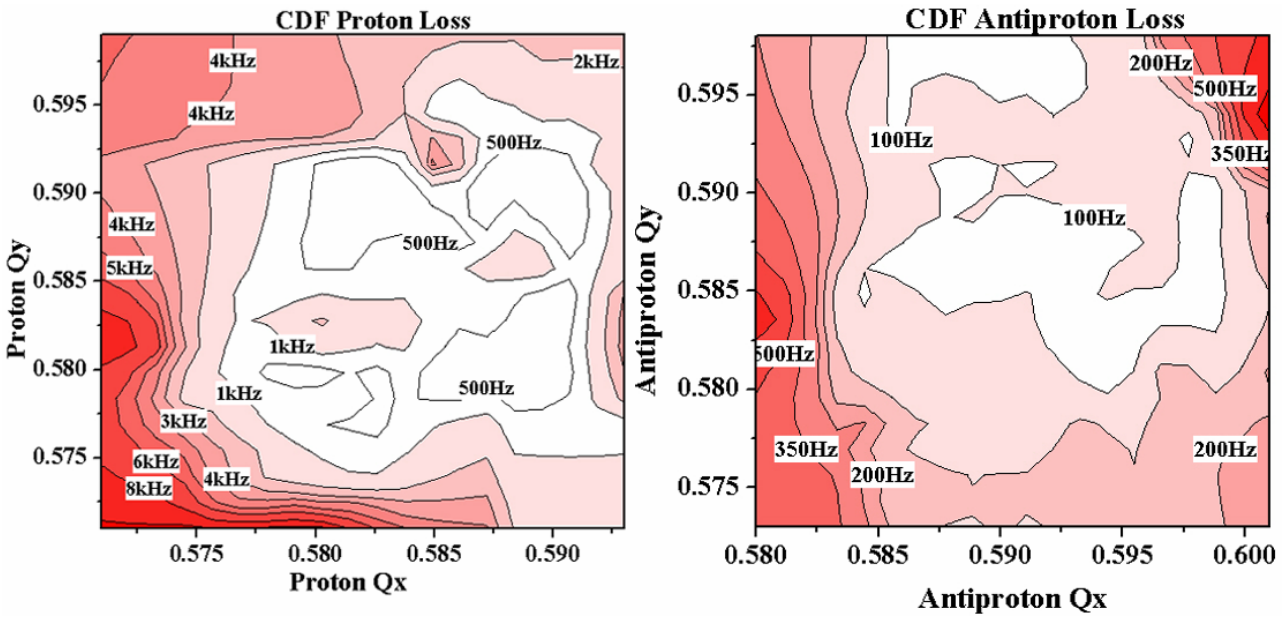

FIG. 32. Contour plots showing background halo rates at the CDF detector for protons (a) and antiprotons (b) vs the measured horizontal and vertical tunes for each beam. The experiment was performed at the end of store #3972 (February 10, 2005). The tunes were measured by the 1.7 GHz Schottky monitor gated on all bunches for each beam.